

Revisiting the second-order convergence of the lattice Boltzmann method with reaction-type source terms

Grzegorz Gruszczyński^{a,b,*}, Michał Dzikowski^b, Łukasz Łaniewski-WoŃk^c

^a*Institute of Aeronautics and Applied Mechanics, Warsaw University of Technology, Warszawa, Poland*

^b*Interdisciplinary Centre for Mathematical and Computational Modelling, University of Warsaw, Warszawa, Poland*

^c*School of Mechanical and Mining Engineering, The University of Queensland, St Lucia, Australia*

Abstract

This study analyses an approach to consistently recover the second-order convergence of the lattice Boltzmann method (LBM), which is frequently degraded by an improper discretisation of the required source terms. The current work focuses on advection-diffusion models, in which the source terms are dependent on the intensity of transported fields. Such terms can be observed in reaction-type equations used in heat and mass transfer problems or multiphase flows. The investigated scheme is applicable to a wide range of formulations within the LBM framework. All considered source terms are interpreted as contributions to the zeroth-moment of the distribution function. These account for sources in a scalar field, such as density, concentration, temperature or a phase field. Further application of this work can be found in the method of manufactured solutions or in the immersed boundary method.

This paper is dedicated to three aspects regarding proper inclusion of the source term in LBM schemes. Firstly, it identifies the differences observed between the ways in which source terms are included in the LBM schemes present in the literature. The algebraic manipulations are explicitly presented in this paper to clarify the observed differences, and to identify their origin. Secondly, it analyses in full detail, the implicit relation between the value of the transported macroscopic field, and the sum of the LBM densities. This relation is valid for any source term discretization scheme. It is a crucial ingredient for preserving the second-order convergence in the case of complex source terms. Moreover, three equivalent forms of the second-order accurate collision operator are presented. Finally, closed form solutions of this implicit relation are shown for a variety of common models, including general linear and second order terms; population growth models, such as the Logistic or Gompertz model and the Allen-Cahn equation.

The second-order convergence of the proposed LBM schemes is verified on both linear and non-linear source terms. The pitfalls of the commonly used acoustic and diffusive scalings are identified and discussed. Furthermore, for a simplified case, the competing errors are shown visually with isolines of error in the space of spatial and temporal resolutions.

Keywords: lattice Boltzmann method, reaction equation, source term, second-order convergence

1. Introduction

The lattice Boltzmann method (LBM) is a widely used numerical scheme for solving both the Navier Stokes equations and advection-diffusion-reaction equation (ADRE). Its popularity has significantly risen in the recent three decades due to its ability to handle complex boundary shapes and its relative ease of implementation and parallelisation. In general, the explicitness of the scheme and the second-order convergence of the LBM is known in the literature [1, 2]. Unfortunately, it may be easily degraded through inconsistent discretisation of the source terms. This may lead to excessive computational requirements to achieve accuracies observed in other formulations.

*Corresponding author.

Email addresses: ggruszczyński@gmail.com (Grzegorz Gruszczyński), mjdzikowski@gmail.com (Michał Dzikowski)

To simplify derivations, the scope of this paper is narrowed to an advection-diffusion-reaction equation,

$$\frac{\partial}{\partial t}\phi + \nabla \cdot (\mathbf{u}\phi) = \nabla \cdot (M\nabla\phi) + Q(\phi, \mathbf{x}, t), \quad (1)$$

where ϕ denotes the scalar field, \mathbf{u} refers to an advection velocity, M is a diffusion coefficient, and Q is the source term. In this work, a consistent discretisation of the source term is discussed in order to recover the second-order convergence of the underlying scheme. The discussion is focused on the situation in which Q is dependent on ϕ itself, i.e., $Q = Q(\phi)$. To the best of the authors' knowledge, such a form has not been analysed in the literature. Integration of the discrete Boltzmann equation (DBE) with trapezoidal rule leads to implicit expressions. To transform them into an explicit scheme, a shift (redefinition) of variables is used [1, 2]. The resulting relation between the macroscopic field, ϕ , and the shifted one, $\tilde{\phi}$, can be expressed as,

$$\phi - \frac{1}{2}Q(\phi, \mathbf{x}, t) = \tilde{\phi}. \quad (2)$$

However, in the case of Q dependent on the ϕ , the Equation (2) is implicit itself and potentially non-linear. The detailed analysis of this issue is the primary concern of the current work. We highlight the often neglected details of the derivation of the LBM in the aforementioned scenario. Next, we exemplify the proper treatment of the implicit, scalar source term in ADRE with an appropriate redefinition of variables and initialisation of the LBM densities.

Finally, we clarify the potential confusion related to the way in which the convergence LBM is investigated. In classical numerical methods, spatial convergence is tested by varying the domain resolution while holding a fine, fixed time step. The idea is to keep the error of temporal discretisation much smaller than the spatial one or vice versa. Due to the relatively narrow range of parameters for which LBM is stable, its convergence is usually investigated for a special relationship between spatial and temporal scales. Usually, these relationships follow the rules of so-called acoustic and diffusive scaling. As a consequence, a biased view of convergence may be reported by looking solely at either spatial or temporal resolution, while the corresponding errors can converge at different rates. The naive discretisation of the source term (assuming $\phi = \tilde{\phi}$) reduces the order of convergence in the case of acoustic scaling. On the other hand, we will demonstrate that the same order of convergence can still be observed even for the improper treatment of the source term under diffusive scaling.

1.1. Discussion on the state of the art

From an application point-of-view, there is a wide range of physical phenomena which can be described by a form of the advection-diffusion-reaction equation. Models based on the LBM were developed for processes such as multicomponent reaction [3], combustion [4], solid and fluid dissolution related to underground CO_2 storage [5, 6], crystallization and melting [7, 8] and heat transfer [1, 9–13]. Last but not least, the numerical solvers can be verified by the method of manufactured solutions [14] in which the source term modelling is extensively used. Selected studies involving the use of LBM are listed below to present both the scope of modelling approaches, and applicability of the concepts discussed in this work.

One of the earliest studies in which the LBM framework was applied to simulate reaction-diffusion equations has been conducted by Dawson et al. [15] in 1993. The group investigated the classical Selkov model (originating from biological studies of glycolysis). They used a hexagonal lattice with a BGK relaxation model and an explicit first-order integration of the source term. The proposed technique was used to simulate pure diffusion, homogenous reaction and the formation of Turing patterns. Later, the model was re-formulated on a square lattice by Blaak and Slood [16]. The first order approximation of the source term was present in both works.

Arguably, the most widely explored application of the advection-diffusion LBM is found in coupled flow-heat transfer problems [1, 9–13]. To model the underlying physics, a two-population approach is frequently used. One of the populations simulates the motion of the fluid, while the second one uses some form of the energy balance equation to resolve the heat transfer. The primary benefit of using the same numerical framework for fluid flow and heat transfer is that it greatly simplifies the computational implementation.

The LBM framework has also been extended to capture the conjugate heat transfer and or phase change between solid and liquid phases. Huang et al. [7, 8] incorporated the term responsible for the latent heat of fusion into the equilibrium distribution function. As a result, moments of equilibrium have been adjusted to recover the desired

partial differential equation. A similar effect has been obtained by Hosseini et al. [17], who presented a set of weight coefficients to tune the second-order moments of a source-like term, which was added to the equilibrium distribution function. Karani and Huber [18], and later Chen et al. [19], studied the macroscopic energy equation suitable to model conjugate heat transfer in comparison with the standard advection-diffusion equation. The difference was expressed as a corrective source term, and was added to the standard LBM routine for the ADRE to obtain the correct energy balance. While the aforementioned works [17–19] introduce a source term specific for conjugate heat transfer problems, they do not discuss its treatment which potentially leads to the use of explicit first-order schemes. Interested readers are referred to a comprehensive review of methods related to phase-change, heat transfer and multiphase flows by Li et al. [20].

The source term technique can be also used to implement a boundary condition on a moving or curved wall. The intensity of the heat source is adjusted in each iteration to match the Dirichlet, Neumann, or Robin boundary condition. Models that use this technique are commonly referred to as immersed boundary method. Seta [21] performed a comprehensive work on its thermal variant, including an analysis of the error terms present. Many authors have recognised the importance of consistently treating the source term with an appropriate scheme [21–27], however, it is not always taken into account [28–30]. An alternative approach to couple the fluid-solid interaction is through the partially saturated method [31], where a lattice node is categorised as a pure fluid, pure solid or mixed one.

To simulate advection-diffusion-reaction in a compressible medium, Aursjø et al. [32] have defined the concentration of the scalar quantity relative to the density of fluid. Later, the same research group proposed a scheme for including a mass source term in the Navier Stokes equations and showed its application for imposing a pressure boundary condition [33].

While problems relating to heat transfer represent the majority of work conducted with the advection-diffusion equation resolved in the LBM framework, other physical phenomena are also studied. When multiple components are present in the same volume, a reaction between them may occur [4, 15, 34, 35]. Kang et al. [34] managed to reduce the number of equations required to solve the problem of dividing species by separating their interaction into reaction rate-, and diffusion-dominated. Again, the convergence was not discussed in [4, 15, 34].

Shi and Guo [36] and Chai et al. [37] provided general studies on the non-linear and anisotropic variants of the advection-diffusion equations in the LBM framework, respectively. The influence of source term treatment is highlighted, but the numerical examples are focused on other aspects of the ADRE and do not include an example of solving non-linear source term preserving both temporal and spatial derivatives. The asymptotic analysis of the LBM schemes for the advection-diffusion equation have been discussed in detail by Yoshida and Nagaoka [38] and Chai and Shi [39]. The authors gave a detailed expansion analysis for both single relaxation time and multiple relaxation time collision operators for the advection-diffusion-reaction system. For the diffusive scaling, second-order accuracy was reported. However, the test cases presented did not include source terms, which were integrated with a first-order scheme.

Having outlined the range of applications, the mathematical methodology is now presented. Readers interested in a detailed discussion on analysis methods are referred to [39–41]. In general, the derivations of the conventional LBM numerical schemes present in the literature, can be broadly divided into two groups. First one is referred as *bottom-up* and the second one as *top-down* approach.

The *bottom-up* procedure starts from an *a priori* postulated discrete evolution scheme. It proceeds with an expansion procedure (such as Chapman-Enskog) to recover the macroscopic equations and to analyse its order of accuracy. Knowing the difference between the target and recovered equation, one can apply corrections to account for the missing terms. Regarding the advection-diffusion-reaction equation, the missing terms are recognised as spatio-temporal derivatives of the source term. To regain second-order accuracy of the numerical scheme, two approaches can be distinguished. Shi et al. [36, 42] evaluated the derivatives using standard finite-difference stencils. On the other hand, Seta [21] and Chai et al. [37] realised that a redefinition of variables allowed the problem to be resolved, while preserving the locality of the underlying scheme. An analogous analysis regarding the forcing term in the Navier Stokes equations have been done by Guo et al. [43].

In the *top-down* approach, the DBE is first constructed. It is then integrated along its characteristics to derive the fully discrete scheme [44–46]. In most cases, the resulting time integration scheme will be implicit. Again, redefinition of variables can be used to transform it into explicit equations [1]. Finally, it is interesting to notice, that some alternative LBM schemes are also being developed [47–49].

1.2. Structure

With the state of the art, and the common methodologies for deriving an LBM scheme introduced, the remainder of this paper is structured as follows. In Section 2.1, a general framework based on a *top-down* approach is discussed in detail. From this, a general method which preserves the second-order nature of the underlying LBM with source terms is analysed. A simplified relaxation procedure using a moment-based collision operator is then presented in Section 2.4.1. Section 3 outlines the non-dimensionalisation procedure for a PDE and the required scaling of parameters on LBM grids. Subsequently, Section 4.1 describes how leading components of error affect the accuracy of a solution in terms of both spatial and temporal resolution. To illustrate the methodology, the proposed approach for solving a formally implicit source term is applied to the Allen-Cahn equation in Section 4.2. With the use of symbolic algebra, a solution with an explicit algorithm, which preserves second-order accuracy is proposed. Finally, the methodology is validated numerically by comparison with a finite-element method solution in Section 4.2.2 and a convergence study is provided in Sections 4.2.1 and 4.2.3. The summary of the findings and major outcomes of this work are presented in Section 5.

Nomenclature

Abbreviations

ADE	advection-diffusion equation
ADRE	advection-diffusion-reaction equation
DBE	discrete Boltzmann equation
FD	finite difference
FEM	finite element method
LBM	lattice Boltzmann method
MRT	multiple relaxation time
ODE	ordinary differential equation
PDE	partial differential equation
SRT	single relaxation time
TRT	two relaxation time

Dimensionless Variables

Da	Damköhler number
Fo	Fourier number
Pe	Péclet number

Superscripts

\sim	redefined (shifted) distribution function or its moment
\star	Post-collision variable
\wedge	Variables from the next time step (t+1)

eq Equilibrium

Symbols

Δt	Temporal resolution (1/T)
Δx	Spatial resolution (1/L)
h_i	<i>i</i> -th distribution function for the ϕ field
\mathbb{M}	Transformation matrix
\mathbb{S}	Relaxation matrix
e	Characteristic lattice velocity
u	Macroscopic velocity vector
x	Position vector
ω_i	<i>i</i> -th relaxation frequency
ϕ	Density of the scalar field
τ	Relaxation time
<i>i</i>	Imaginary number
Υ_i	<i>i</i> -th raw moment of the distribution function
c_s	Lattice speed of sound
L	Number of lattice elements per length
M	Macroscopic diffusion coefficient
Q	Macroscopic source term
T	Number of time iterations (time steps)

2. Model description

2.1. Discrete Boltzmann equation (DBE)

Here, the iterative scheme is derived using the *top-down* approach, i.e. by direct integration of the DBE. For a set of densities $h_i(\mathbf{x}, t)$, and velocity vectors \mathbf{e}_i , the DBE is known as ([2, Chapter 3.4 and 8.3]),

$$\frac{\partial}{\partial t} h_i + e_i^j \frac{\partial}{\partial x_j} h_i = \frac{1}{\tau} (h_i^{\text{eq}}(\phi, \mathbf{u}) - h_i) + q_i(\phi, \mathbf{x}, t), \quad (3)$$

where h^{eq} is the equilibrium distribution, q is the source term, $\phi = \sum_i h_i$ is the scalar field, and \mathbf{u} is the advection velocity. It is important to reiterate here that the source term depends on the investigated scalar field. With an appropriate choice of equilibrium distribution [2], this equation can be shown to represent the advection-diffusion-reaction equation with, $\phi = \sum_i h_i$, and $Q = \sum q_i$. The equations for the equilibrium distribution are presented in Section 2.4. An important property of the equilibrium that will be used, is,

$$\sum_i h_i^{\text{eq}}(\phi, \mathbf{u}) = \phi. \quad (4)$$

Contrary to classical numerical methods, such as finite-volume or finite-element method, the space and time integration can not be treated independently in the construction of a conventional LBM scheme. For a fixed i , x and t , the characteristic of DBE is given by $\mathbf{x}(s) = \mathbf{x} + s \mathbf{e}_i$, and $t(s) = t + s$. Integrating over s from 0 to 1 we get,

$$\underbrace{\int_0^1 \left(\frac{\partial}{\partial t} h_i + e_i^j \frac{\partial}{\partial x_j} h_i \right) ds}_{I_1} = \underbrace{\int_0^1 \left(\frac{1}{\tau} (h_i^{\text{eq}} - h_i) + q_i \right) ds}_{I_2}. \quad (5)$$

Two integrals, I_1 and I_2 , can be identified in the integration process of the DBE. To denote the variables from the next time step, the hat superscript is used in this work. Namely, $\hat{\mathbf{x}} = \mathbf{x} + \mathbf{e}_i$, $\hat{t} = t + 1$, $\hat{\phi} = \phi(\hat{\mathbf{x}}, \hat{t})$ and $\hat{\mathbf{u}} = \mathbf{u}(\hat{\mathbf{x}}, \hat{t})$. The first integral can be evaluated directly, as it is a material derivative of h_i ,

$$I_1 = \int_0^1 \left(\frac{\partial}{\partial t} h_i + e_i^j \frac{\partial}{\partial x_j} h_i \right) ds = h_i(\hat{\mathbf{x}}, \hat{t}) - h_i(\mathbf{x}, t). \quad (6)$$

The second integral can be approximated by the trapezoidal rule,

$$\begin{aligned} I_2 &= \int_0^1 \left(\frac{1}{\tau} (h_i^{\text{eq}} - h_i) + q_i \right) ds \\ &\simeq \frac{1}{2} \left[\frac{1}{\tau} (h_i^{\text{eq}}(\hat{\phi}, \hat{\mathbf{u}}) - h_i(\hat{\mathbf{x}}, \hat{t})) + q_i(\hat{\phi}, \hat{\mathbf{x}}, \hat{t}) + \frac{1}{\tau} (h_i^{\text{eq}}(\phi, \mathbf{u}) - h_i(\mathbf{x}, t)) + q_i(\phi, \mathbf{x}, t) \right]. \end{aligned} \quad (7)$$

Integrating Equation (7) over the characteristics, and collecting the variables from the next time step (which depend on $\hat{\mathbf{x}}$ and \hat{t}) on the left hand side gives,

$$\underbrace{\left[1 + \frac{1}{2\tau} \right] h_i(\hat{\mathbf{x}}, \hat{t}) - \frac{1}{2\tau} h_i^{\text{eq}}(\hat{\phi}, \hat{\mathbf{u}}) - \frac{1}{2} q_i(\hat{\phi}, \hat{\mathbf{x}}, \hat{t})}_{\text{Equation (9)}} = \left[1 - \frac{1}{2\tau} \right] h_i(\mathbf{x}, t) + \frac{1}{2\tau} h_i^{\text{eq}}(\phi, \mathbf{u}) + \frac{1}{2} q_i(\phi, \mathbf{x}, t). \quad (8)$$

Next, a shifted distribution, \tilde{h} , is introduced to remove the implicit relation from Equation (8). To illustrate the idea, a simple example of variable shift in a ordinary differential equation is presented in [Appendix A](#). A general description of this procedure in the contexts of LBM can be found in the textbook by Krüger et al. [2, Chapter 3.5]).

The new (shifted) distribution, denoted with a tilde, is defined as,

$$\tilde{h}_i(\bullet) = \left[1 + \frac{1}{2\tau}\right] h_i(\bullet) - \frac{1}{2\tau} h_i^{eq}(\bullet) - \frac{1}{2} q_i(\bullet) \quad (9)$$

$$\implies h_i(\bullet) = \frac{1}{1 + \frac{1}{2\tau}} \left(\tilde{h}_i(\bullet) + \frac{1}{2\tau} h_i^{eq}(\bullet) + \frac{1}{2} q_i(\bullet) \right), \quad (10)$$

where \bullet is a placeholder for variables in either t or \hat{t} . Substituting Equation (9) into the left-hand side of Equation (8) and Equation (10) into the right-hand side of Equation (8) leads to a fully explicit evolution scheme (see [Appendix B](#) for details),

$$\tilde{h}_i(\mathbf{x} + \mathbf{e}_i, t + 1) = \tilde{h}_i^*(\mathbf{x}, t) = (1 - \omega) \tilde{h}_i(\mathbf{x}, t) + \omega h_i^{eq}(\phi, \mathbf{u}) + \left(1 - \frac{\omega}{2}\right) q_i(\phi, \mathbf{x}, t), \quad (11)$$

where a relaxation frequency, $\omega = \frac{1}{\tau + 1/2}$, has been introduced to simplify the expression. The post-collision densities are denoted as \tilde{h}^* . It is important to underline, that \tilde{h} is the variable solved in the implementation of a LBM scheme, and is denoted with a tilde in this paper to distinguish it from the non-shifted population, h . The differences in the discretisation schemes available in the literature are discussed in [Appendix C](#).

2.2. Calculation of the scalar field

Equation (11) would be an explicit iterative scheme for \tilde{h} , if not for the implicit dependence on the scalar field, ϕ . One can calculate ϕ from \tilde{h} by summation of Equation (9) noting that both $\sum_i h_i$ and $\sum_i h_i^{eq}$ are equal to ϕ ,

$$\begin{aligned} \tilde{\phi} &= \sum_i \tilde{h}_i = \left(1 + \frac{1}{2\tau}\right) \sum_i h_i(\mathbf{x}, t) - \frac{1}{2\tau} \sum_i h_i^{eq}(\phi, \mathbf{u}) - \frac{1}{2} \sum_i q_i(\phi, \mathbf{x}, t) \\ &= \left(1 + \frac{1}{2\tau}\right) \phi - \frac{1}{2\tau} \phi - \frac{1}{2} Q(\phi, \mathbf{x}, t) \\ &= \phi - \frac{1}{2} Q(\phi, \mathbf{x}, t). \end{aligned} \quad (12)$$

Since the source term depends on the scalar field, $Q = Q(\phi, \mathbf{x}, t)$, one must solve the implicit equation for ϕ to retain the second-order convergence of the underlying scheme. This can be done with a sub-iteration routine, such as bisection or Newton's method, and in certain cases it can be solved analytically. In [Table 1](#), a set of common source terms is presented with corresponding equations for the scalar field, ϕ . In some cases multiple solutions to the implicit equation can exist, and physical limitations must be applied to select the appropriate value. For these cases, the relevant conditions are listed in the notes. If Q is dependent only on the spatial, \mathbf{x} , and temporal, t , location, the equation reduces to, $\phi = \tilde{\phi} + \frac{1}{2} Q(\mathbf{x}, t)$, which is commonly encountered in the literature.

Observe, that the equation for the macroscopic quantity, ϕ , is independent of the LBM scheme being used. Namely, for any collision operator, for example single relaxation time, multiple relaxation time or cascaded LBM, and any discretisation of the source term, q_i , the equation will stay the same.

2.3. Initialization

As the densities simulated in the LBM are different than the DBE densities, the difference must to be taken into account in the initialization procedure. Namely, if one assumes the DBE to be initialized by the equilibrium distribution function, the LBM densities need to be initialized as,

$$\begin{aligned} \tilde{h}_i(x, 0) &= h_i^{eq}(\phi_0, \mathbf{u}_0) - \frac{1}{2} q_i(\phi_0, x, 0) \\ &= h_i^{eq}(\tilde{\phi}_0, \mathbf{u}_0), \end{aligned} \quad (13)$$

Table 1: Calculation of the value of the macroscopic scalar field ϕ from the sum of LBM densities $\tilde{\phi} = \sum_i \tilde{h}_i$. In cases of higher order terms, only one branch of the implicit function is selected, based on physical considerations.

Class	Source term	Equation for ϕ	Notes
No source term	$Q = 0$	$\phi = \tilde{\phi}$	
ϕ independent term	$Q = Q(x, t)$	$\phi = \tilde{\phi} + \frac{1}{2}Q(x, t)$	
General 1st order term	$Q = -\lambda(\phi - \gamma)$	$\phi = \tilde{\phi} + \frac{1}{2+\lambda}\lambda(\gamma - \tilde{\phi})$	
Linear decay	$Q = -\lambda\phi$	$\phi = \frac{2}{2+\lambda}\tilde{\phi}$	
General 2nd order term	$Q = -\lambda(\phi^2 - B\phi + C)$	$\phi = \alpha + \sqrt{\frac{2}{\lambda}\tilde{\phi} + \alpha^2 - C}$	for $\phi > \alpha$, where $\alpha = \frac{B}{2} - \frac{1}{\lambda}$
Logistic model	$Q = \lambda\phi(1 - \frac{\phi}{\gamma})$	$\phi = \alpha + \sqrt{\frac{2\gamma}{\lambda}\tilde{\phi} + \alpha^2}$	for $\phi > \alpha$, where $\alpha = \gamma(\frac{1}{2} - \frac{1}{\lambda})$
Gompertz model	$Q = -\lambda\phi \ln \frac{\phi}{\gamma}$	$\phi = \alpha e^{\mathcal{W}_0(\frac{2}{\lambda}\frac{\tilde{\phi}}{\alpha})}$	for $\phi > \alpha e^{\frac{1}{e}}$, where $\alpha = \gamma e^{-\frac{1}{e}}$, and \mathcal{W} is the Lambert W function
Allen-Cahn equation	$Q = \lambda\phi(1 - \phi^2)$	$\phi = \frac{A}{C} - C$	for $\lambda < 2$, where $A = \frac{2-\lambda}{3\lambda}$, $B = \frac{\phi}{\lambda}$, and $C = \sqrt[3]{\sqrt{B^2 + A^3} - B}$
General term	$Q = Q(\phi, x, t)$	$\phi - \frac{1}{2}Q(\phi, x, t) = \tilde{\phi}$	implicit equation, which can be solved with sub-iterations

where ϕ_0 and \mathbf{u}_0 are the initial values of the macroscopic field and advection velocity respectively. Taking advantage of Equation (12), the initialization procedure can be simplified by calculating $\tilde{\phi}_0$. Omission of this crucial adjustment of the initialization procedure will result in a solution inconsistent with the desired initial condition, and will reduce the order of convergence. Note, that Equation (13) gives the value of the initial distribution functions after streaming and before collision.

2.4. Moments of the distribution

In order to formally discuss different LBM schemes, the concept of moments of the distribution is introduced in this section. Here, the D2Q9 lattice will be adopted for illustrational purposes, but without the loss of generality. The D2Q9 is the most popular lattice discretisation used for 2D problems, and it defines the discrete velocity vectors \mathbf{e}_i as,

$$\begin{aligned}
 \mathbf{e}_1 &= [0, 0] & \mathbf{e}_2 &= [1, 0] & \mathbf{e}_3 &= [0, 1] \\
 \mathbf{e}_4 &= [-1, 0] & \mathbf{e}_5 &= [0, -1] & \mathbf{e}_6 &= [1, 1] \\
 \mathbf{e}_7 &= [-1, 1] & \mathbf{e}_8 &= [-1, -1] & \mathbf{e}_9 &= [1, -1]
 \end{aligned}$$

The discrete, raw moments in 2D are defined as,

$$\Upsilon_{mn} = \sum_i (e_i^x)^m (e_i^y)^n h_i, \quad (14)$$

which can be easily extended to 3D with three indices. For moments of LBM densities, \tilde{h} , post-collision densities, \tilde{h}_i^\star , equilibrium distribution, h^{eq} and source term, q , we will use $\tilde{\Upsilon}$, $\tilde{\Upsilon}^\star$, Υ^{eq} and \mathbf{R} respectively.

As the set of densities is finite, and the velocities \mathbf{e} are distinct, one can select a finite set of linearly independent moments to fully represent any set of densities. For the D2Q9 lattice, the following set of moments is chosen,

$$\Upsilon = [\Upsilon_{00} \quad \Upsilon_{10} \quad \Upsilon_{01} \quad \Upsilon_{20} \quad \Upsilon_{02} \quad \Upsilon_{11} \quad \Upsilon_{21} \quad \Upsilon_{12} \quad \Upsilon_{22}]^T. \quad (15)$$

The transformation from the densities, h , to the vector of moments can be expressed through matrix multiplication as $\Upsilon = \mathbb{M}h$. In the case of D2Q9, this matrix reads,

$$\mathbb{M} = \begin{bmatrix} 1 & 1 & 1 & 1 & 1 & 1 & 1 & 1 & 1 \\ 0 & 1 & 0 & -1 & 0 & 1 & -1 & -1 & 1 \\ 0 & 0 & 1 & 0 & -1 & 1 & 1 & -1 & -1 \\ 0 & 1 & 0 & 1 & 0 & 1 & 1 & 1 & 1 \\ 0 & 0 & 1 & 0 & 1 & 1 & 1 & 1 & 1 \\ 0 & 0 & 0 & 0 & 0 & 1 & -1 & 1 & -1 \\ 0 & 0 & 0 & 0 & 0 & 1 & 1 & -1 & -1 \\ 0 & 0 & 0 & 0 & 0 & 1 & -1 & -1 & 1 \\ 0 & 0 & 0 & 0 & 0 & 1 & 1 & 1 & 1 \end{bmatrix}. \quad (16)$$

It is convenient to express LBM schemes in terms of moments, and not densities themselves. This is because they represent specific mechanics, and or have physical interpretations, which the densities themselves do not possess. The LBM collision operator defined in equation Equation (11), can be expressed using moments as,

$$\tilde{\Upsilon}^*(\mathbf{x}, t) = (1 - \omega)\tilde{\Upsilon}(\mathbf{x}, t) + \omega\Upsilon^{\text{eq}}(\phi, \mathbf{u}) + \left(1 - \frac{\omega}{2}\right)\mathbf{R}(\phi, \mathbf{u}, \mathbf{x}, t). \quad (17)$$

The moments of the discrete equilibrium, Υ^{eq} , are defined to be equal to moments of the continuous Maxwell-Boltzmann distribution function, $\Upsilon^{\text{eq}}(\phi, \mathbf{u}) = \phi \Gamma(\mathbf{u})$, where,

$$\Gamma(\mathbf{u}) = \left[1 \quad u_x \quad u_y \quad c_s^2 + u_x^2 \quad c_s^2 + u_y^2 \quad u_x u_y \quad u_y(c_s^2 + u_x^2) \quad u_x(c_s^2 + u_y^2) \quad c_s^4 + c_s^2(u_x^2 + u_y^2) + u_x^2 u_y^2\right]^\top. \quad (18)$$

One can clearly see that these moments fulfil the conditions required for representation of the advection-diffusion-reaction equation by the DBE. A common choice of the speed of sound c_s is $1/\sqrt{3}$, which reduces the error in higher moments. The moments of the equilibrium distribution are truncated by some authors on the second order terms [1, 7, 9, 10], by not including the terms $u_x^2 u_y$, $u_x u_y^2$ and $u_x^2 u_y^2$. Furthermore, it can be truncated at first-order terms [17–19, 38] giving,

$$\Gamma^{\text{1st order}}(\mathbf{u}) = \left[1 \quad u_x \quad u_y \quad c_s^2 \quad c_s^2 \quad 0 \quad u_y c_s^2 \quad u_x c_s^2 \quad c_s^4\right]^\top. \quad (19)$$

Formulas analogous to Equation (18) can be used for the D2Q5 lattice [12]. Similarly, the moments of the source term can be expressed as $\mathbf{R} = Q(\phi, \mathbf{x}, t) \Gamma(\mathbf{u})$. Again, some authors simplify the source term by truncating the velocity [38, 50]. Investigation of an error related to the order of velocity expansion of the equilibrium distribution function has been conducted by Chopard et al. [51]. It has been shown that the full order velocity expansion enhances both the Galilean invariance [11, 52–54] and stability of the LBM schemes [52, 54].

The equilibrium and source term distribution functions can be easily calculated from their moments as $\mathbf{h}^{\text{eq}} = \mathbb{M}^{-1}\Upsilon^{\text{eq}}$ and $\mathbf{q} = \mathbb{M}^{-1}\mathbf{R}$.

2.4.1. The collision operator

If the moments of the source term are chosen to be $\mathbf{R} = Q(\phi, \mathbf{x}, t) \Gamma(\mathbf{u})$, and $\Upsilon^{\text{eq}}(\phi, \mathbf{u}) = \phi \Gamma(\mathbf{u})$, one can use Equations (12) and (18) to express the collision operator in three equivalent forms,

$$\tilde{\Upsilon}^* = (1 - \omega)\tilde{\Upsilon} + \omega\Upsilon^{\text{eq}}(\phi, \mathbf{u}) + \left(1 - \frac{\omega}{2}\right)\mathbf{R} \quad (20)$$

$$= (1 - \omega)\tilde{\Upsilon} + \omega\Upsilon^{\text{eq}}(\tilde{\phi}, \mathbf{u}) + \mathbf{R} \quad (21)$$

$$= (1 - \omega)\left(\tilde{\Upsilon} - \Upsilon^{\text{eq}}(\tilde{\phi}, \mathbf{u})\right) + \Upsilon^{\text{eq}}(\tilde{\phi} + Q, \mathbf{u}). \quad (22)$$

The form provided in Equation (21) can be viewed as a simplification of a relaxation procedure expressed in central moments space by Fei and Luo [12]. On the other hand, the form in Equation (22) can be interpreted as a natural extension of the exact difference method [55] for reaction-type source terms. Even though Equations (21) and (22)

use $\Upsilon^{\text{eq}}(\tilde{\phi}, \mathbf{u})$ instead of $\Upsilon^{\text{eq}}(\phi, \mathbf{u})$, the implicit Equation (12) must still be resolved as the source term Q is dependent on ϕ .

For a comparison of forcing schemes, the reader is referred to the studies [43, 56]. Further discussion concerning discretisation and the order of the velocity expansion of the forcing scheme in the central moment space can be found in [57–59] and references therein.

2.4.2. Two relaxation time

The two relaxation time (TRT) collision operator was shown to have superior accuracy and stability [60, 61] when compared to the single relaxation time collision presented in the previous section. The TRT approach consists of decomposing the distribution function into symmetric and anti-symmetric components [60],

$$h_j^{\text{even}} = \frac{h_j + h_k}{2}, \quad (23a)$$

$$h_j^{\text{odd}} = \frac{h_j - h_k}{2}, \quad (23b)$$

for k chosen such that $\mathbf{e}_j = -\mathbf{e}_k$. For the two components, two different relaxation times, τ , are used resulting in two different relaxation coefficients, ω .

The symmetric component, h_j^{even} , has only even order moments, and the anti-symmetric component has only odd order moments that are non-zero. This means that a TRT collision can be constructed from Equation (21) as,

$$\tilde{\Upsilon}^* = (1 - \mathbb{S})\tilde{\Upsilon} + \mathbb{S}\Upsilon^{\text{eq}}(\tilde{\phi}, \mathbf{u}) + \mathbf{R}, \quad (24)$$

where \mathbb{S} is the diagonal relaxation matrix, which has ω_{odd} in rows corresponding to moments of odd order, and ω_{even} otherwise. For D2Q9 the matrix is as follows,

$$\mathbb{S} = \text{diag}([\omega_{\text{even}}, \omega_{\text{odd}}, \omega_{\text{odd}}, \omega_{\text{even}}, \omega_{\text{even}}, \omega_{\text{even}}, \omega_{\text{odd}}, \omega_{\text{odd}}, \omega_{\text{even}}]). \quad (25)$$

This means that the non-orthogonal matrix of raw moments, \mathbb{M} , provided in Equation (16), diagonalises the TRT collision operator [62]. For additional information on the TRT method, the interested reader is directed to the work of Ginzburg [60], although this particular property has not been explicitly stated there. In case of the advection-diffusion equation, the relaxation rate for odd moments, ω_{odd} , has to correspond to the macroscopic diffusion coefficient,

$$\omega_{\text{odd}} = \frac{1}{\frac{M}{c_s^2} + 1/2}. \quad (26)$$

On the other hand, the (tunable) relaxation rate for even moments, ω_{even} , can be defined based on the so-called magic parameter,

$$\Lambda = \left(\frac{1}{\omega_{\text{odd}}} - \frac{1}{2} \right) \left(\frac{1}{\omega_{\text{even}}} - \frac{1}{2} \right). \quad (27)$$

Fixing the magic parameter at different constant values, results in a minimisation of specific types of discretisation errors, and can improve stability and or accuracy of commonly used boundary conditions [60, 61].

2.4.3. Streaming

As usual, the collision step, given by Equation (24), is followed by the streaming step,

$$\tilde{h}_i(\mathbf{x} + \mathbf{e}_i, t + 1) = \tilde{h}_i^*(\mathbf{x}, t) = \mathbb{M}^{-1}\tilde{\Upsilon}^*(\mathbf{x}, t). \quad (28)$$

Concluding, the order of operations in the LBM scheme can be presented as in Figure 1.

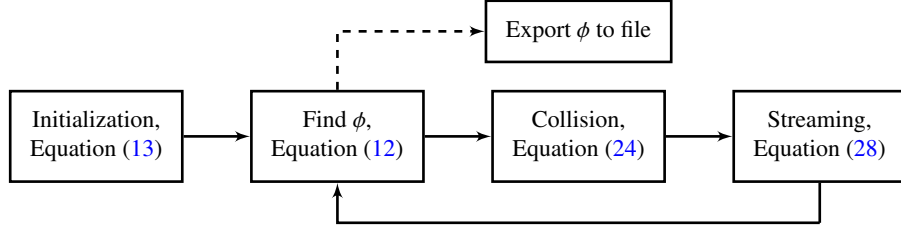


Figure 1: The order of operations performed during execution of the solver.

3. Scaling of LBM

To represent the same physical problem, the non-dimensional form of the investigated differential equation must be preserved on a set of LBM grids. Let us consider a source term $Q = \lambda P(\phi)$, where P has the same unit as ϕ , and λ is a scaling coefficient (see Table 1). Using L , T and U as reference length, time and velocity, respectively, one can define non-dimensional coordinates $x = x^*L$, $t = t^*T$, $u = u^*U$. For a constant M one can express the Equation (1) in non-dimensional form [63],

$$\frac{\partial}{\partial t^*} \phi + \mathbf{Pe} \mathbf{Fo} \nabla^* \cdot (\mathbf{u}^* \phi) = \mathbf{Fo} \Delta^* \phi + \mathbf{Da} \mathbf{Fo} P(\phi), \quad (29)$$

where \mathbf{Fo} , \mathbf{Da} and \mathbf{Pe} are dimensionless numbers:

- Fourier number $\mathbf{Fo} = \frac{MT}{L^2}$ — the ratio of the diffusive term to the temporal term;
- (second) Damköhler number $\mathbf{Da} = \frac{\lambda L^2}{M}$ — the ratio of the reaction term to the diffusive term;
- Péclet number $\mathbf{Pe} = \frac{UL}{M}$ — the ratio of the convective term to the diffusive term.

Observe, that the Fourier number incorporates the temporal scale of the simulation and as such can be considered as a non-dimensional time. An alternative approach would be to fix $\mathbf{Fo} = 1$, and quote the time of simulation for each case.

The LBM grids are described by their characteristic length and time (L, T) expressed in number of elements and time-steps. The element size, and time-step can be expressed as their inverse, $\Delta x = \frac{1}{L}$ and $\Delta t = \frac{1}{T}$. For each grid, there are corresponding values of M , λ , and U that preserve the dimensionless numbers: $M = \mathbf{Fo} \frac{L^2}{T}$, $\lambda = \mathbf{Da} \mathbf{Fo} \frac{1}{T}$ and $U = \mathbf{Pe} \mathbf{Fo} \frac{L}{T}$.

For the so-called acoustic scaling, one uses a series of lattices with $L_k = \varepsilon_k^{-1} L_0$ and $T_k = \varepsilon_k^{-1} T_0$, for some scaling factor $\varepsilon_k \rightarrow 0$. Using the previously mentioned equations for the simulation parameters one obtains, $M_k = \varepsilon_k^{-1} M_0$, $U_k = U_0$, and $\lambda_k = \varepsilon_k \lambda_0$. This scaling is called acoustic, as it preserves the velocity scale, making the speed of sound constant across the series of LBM grids. On the other hand, for diffusive scaling, one has $L_k = \varepsilon_k^{-1} L_0$ and $T_k = \varepsilon_k^{-2} T_0$. This in turn gives, $M_k = M_0$, $U_k = \varepsilon_k U_0$, and $\lambda_k = \varepsilon_k^2 \lambda_0$. This scaling is called diffusive, as the diffusion coefficient M is constant across the series of LBM grids.

4. Model Verification and Validation

To test the numerical properties of the described LBM scheme, two equations were investigated, an advection diffusion equation, with a linear source term, and the Allen-Cahn equation. As analytical solutions are easy to obtain for the first example, a detailed analysis of error is performed in that case. Also, for the first equation, the results are compared with the situation in which one would naively assume $\phi = \tilde{\phi}$. In the case of the Allen-Cahn equation, which has a bi-stable, highly non-linear source term, convergence is checked for both uniform, and non-trivial initial conditions.

If not stated differently, the error between the numerical solution $\phi(x_i)$ defined on the lattice points x_i and the reference solution ϕ_{ref} is quantified using the \mathcal{L}_2 norm, defined as:

$$\mathcal{L}_2 \text{ norm of error} = \sqrt{\frac{1}{N} \sum_{i=1}^N (\phi(x_i) - \phi_{\text{ref}}(x_i))^2}, \quad (30)$$

where N is the number of points in the lattice.

4.1. Linear advection-diffusion-reaction model

Here, a simple equation with a linear source term is considered,

$$\frac{\partial \phi}{\partial t} + \nabla \cdot (\mathbf{u}\phi) = \nabla \cdot (M\nabla \phi) + \underbrace{\lambda(\eta(\mathbf{x}) - \phi)}_{Q=Q(\phi)}, \quad (31)$$

where λ is a constant and $\eta(\mathbf{x})$ is a known function. On a periodic domain with constant velocity, \mathbf{u} , the problem is a first order linear differential equation, which acts independently on all wavelengths. That means that for any selected wavevector \mathbf{k} , we can solve analytically the equation for initial condition $\phi|_{t=0} = Pe^{i\mathbf{k}\cdot\mathbf{x}}$ and $\eta = Ge^{i\mathbf{k}\cdot\mathbf{x}}$, where upright i denotes the imaginary unit. The analytical solution will be a transition between the initial condition and the steady state,

$$\phi_{\text{analytical}}(\mathbf{x}, t) = \left(e^{-at}P + (1 - e^{-at})a^{-1}\lambda G \right) e^{i\mathbf{k}\cdot\mathbf{x}}, \quad (32)$$

where $a = \lambda + i(\mathbf{u} \cdot \mathbf{k}) + M(\mathbf{k} \cdot \mathbf{k})$. As the equation is linear, one can take the imaginary or real part of the above analytical solution to obtain a real valued solution. If not specifically mentioned, the real part is used in tests. By varying P and G one can study the influence of the initial condition and the steady-state solution respectively.

4.1.1. Second-order convergence

To test the convergence, the Equation (31) was solved on a periodic domain of size $L \times L$ elements for a time t with $\mathbf{Fo} = 0.001$ and $\mathbf{Da} = 1000$. In all computations of this case, the single relaxation time collision operator was used. The number of time steps was increased by a factor of 2 from $T = 2^9$ to $T = 2^{15}$, while maintaining the number of elements per length, L , proportional such that $16L = T$ (acoustic scaling). The velocity was varied between $\mathbf{Pe} = 0$ and $\mathbf{Pe} = 1000$ and the wave number k was $0\frac{2\pi}{L}$, $1\frac{2\pi}{L}$ or $2\frac{2\pi}{L}$. For each setup, two cases were executed. One with $P = 1$ and $G = 0$, and the other with $P = 0$ and $G = 1$. The LBM solutions were compared with the analytical solution of Equation (31), and the \mathcal{L}_2 norm of the difference was computed. The proposed scheme consistently recovered second-order convergence for all the cases, with the slope varying from 1.99 to 2.2 as calculated with a least square fit. Figure 2 provides an indication of the convergence for $k = 1\frac{2\pi}{L}$, $P = 1$ and $G = 0$. The convergence observed was compared to results obtained when ignoring the implicit Equation (12) and assuming $\phi = \tilde{\phi}$ in the calculation of Q .

4.1.2. Convergence of DBE to ADRE

The LBM can be treated as a discretisation of the DBE, which in turn converges to the ADRE that one originally wanted to solve. This means that two types of error need to be considered, namely, the error of discretisation, and the error (difference) between the DBE and ADRE. Readers interested in a more detailed study regarding equivalent partial differential equations for the lattice Boltzmann schemes are referred to the recent work of Fučík and Straka [40] and Simonis et al. [41].

In the case of the linear source term, $\mathbf{q} = Q(\phi)\boldsymbol{\gamma}(\mathbf{u})$, $\mathbf{h}^{\text{eq}} = \phi\boldsymbol{\gamma}(\mathbf{u})$ and $\boldsymbol{\gamma}(\mathbf{u}) = \mathbb{M}^{-1}\boldsymbol{\Gamma}(\mathbf{u})$; see Equation (18) for the definition of $\boldsymbol{\Gamma}(\mathbf{u})$. Assuming an uniform velocity field, \mathbf{u} , the DBE given in Equation (3) can be solved analytically and its solution can be conveniently expressed using matrix exponents,

$$\mathbf{h}_{\text{analytical}}^{\text{DBE}}(\mathbf{x}, t) = \left(e^{-A t} \boldsymbol{\gamma}(\mathbf{u}) P + (I - e^{-A t}) A^{-1} \boldsymbol{\gamma}(\mathbf{u}) \lambda G \right) e^{i\mathbf{k}\cdot\mathbf{x}}, \quad (33)$$

where $A_{jk} = i\delta_{jk}(\mathbf{e}_j \cdot \mathbf{k}) - \frac{1}{\tau}(\gamma_j(\mathbf{u}) - \delta_{jk}) + \lambda\gamma_j(\mathbf{u})$. Substitution of all variables indicates that the analytical solution of the ADRE is independent of L and T , as one would expect, however, the analytical solution of the DBE is only dependent on ratio of L to T (the velocity scale).

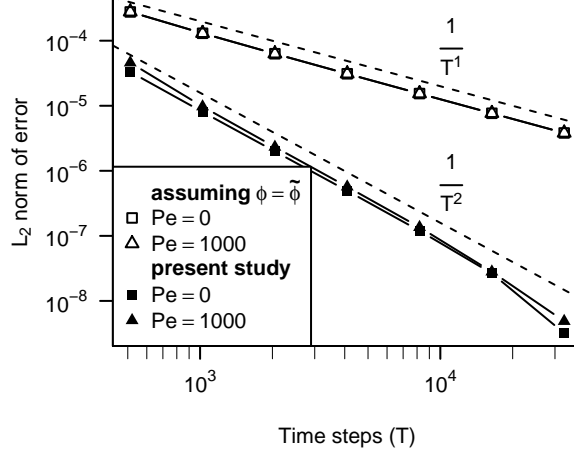


Figure 2: Convergence of the solution of Equation (31) compared with analytical solution given by Equation (32), for $k = 1 \frac{2\pi}{L}$, $P = 1$ and $G = 0$.

Figure 3 provides the \mathcal{L}_2 norm of the difference between the complex solutions of DBE and ADRE. The two components of the error can be observed, namely, the fourth-order, velocity dependent error, and second-order, velocity independent error.

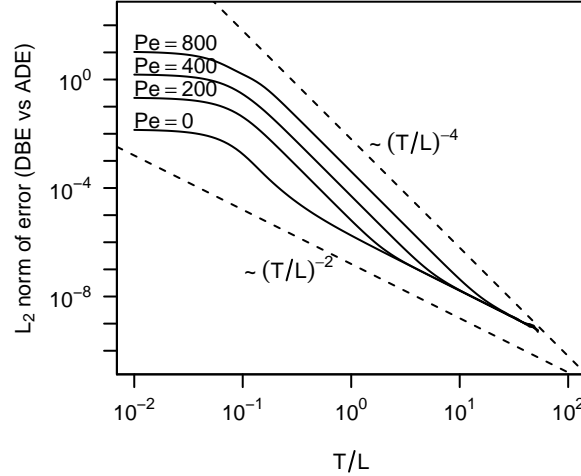


Figure 3: \mathcal{L}_2 norm of the difference between the analytical solutions of the discrete Boltzmann Equation (3) and the advection-diffusion-reaction Equation (1). Evaluated for $k = 1 \frac{2\pi}{L}$, $M = 0.001 \frac{L^2}{T}$, $G = 0$, and $P = 1$.

4.1.3. Error landscape

A better understanding of the behaviour of the LBM method for the advection-diffusion-reaction equation, and LBM in general, can be gained by looking at the dependence of the error on both spatial and temporal resolution. In this work, this is termed the error landscape. For most physical problems it is prohibitively expensive to calculate the full error landscape, even if an analytical solutions is available. Nevertheless, the landscape for this case is discussed here, as the general trends and slopes of this landscape will be similar in any LBM application.

A set of 23 and 31 distinct values of L and T were selected, generating a solution set that is close to a linear distribution in log space. For each pair, two simulations were performed, one with the method presented in this paper, and one in which Q is calculated from $\tilde{\phi}$, not ϕ . In total, 1426 simulations were performed to populate the error landscape. The results were compared to both the analytical solutions of the ADRE and DBE. Figure 4 presents

the isolines of the error. One can observe, that the convergence to the DBE is only driven by competing temporal

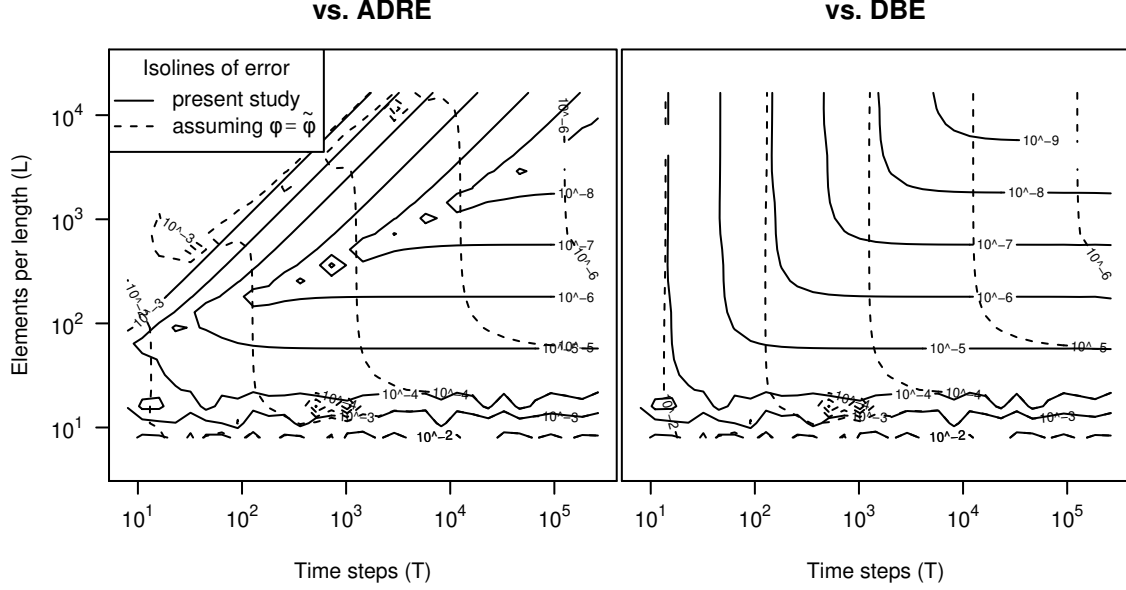


Figure 4: The isolines of error of the LBM solution against advection-diffusion-reaction equation and discrete Boltzmann equation, given by Equation (32) and Equation (33), in the T-L space. The y-axis of the left-hand and right-hand side plots are the same. Error is defined as \mathcal{L}_2 -norm of the difference between LBM solution and the reference one. All combinations of 23 and 31 distinct values of L and T respectively, were simulated. Evaluated for $k = \frac{2\pi}{L}$, $M = 0.001 \frac{L^2}{T}$, $G = 0$, $P = 1$, and $u = 0$.

and spatial discretisation errors. On the other hand, the T/L dependent error between DBE and ADRE dominates the temporal error in convergence to ADRE. In either case, if the source term is inappropriately integrated, its first-order error reduces the accuracy greatly in almost the entire landscape (marked with dashed lines).

In order to provide a clear view of the trends present in the error landscape, approximations of all the separate errors were established to create a smoothed landscape presented in Figure 5. To quantify the impact of the source term discretisation, the computational cost was compared to achieve the same level of error using either a first- or second-order scheme. Both for the present method, and for the inconsistent integration, an optimal selection of number of time-steps, T , and number of elements, L , was made, to achieve an error of no more than 10^{-5} . In this specific example, the use of the inconsistent integration scheme for the source term leads to an increase in computational effort (L^2T) of the factor of 500 to achieve an equivalent level error.

The landscapes presented in Figures 4 and 5 indicate the pitfalls of analysing the convergence of LBM. It has to be reiterated that the Boltzmann equation is integrated along the characteristics, thus the space and time integration can not be treated independently in the construction of a conventional LBM scheme. As a consequence, a properly implemented LBM scheme has second-order convergence. The isolines of error, presented in Figure 5, are commonly traversed along the directions marked by the acoustic and diffusive scaling. Given a specific scaling, i.e. ratio of temporal to spatial resolution between subsequent refinements, a researcher may get a biased view of the error and the order of convergence. For instance, under the diffusive scaling, a second order convergence in space will be observed for both the trapezoidal and Euler's implementation of the reaction term integrator. An example of first order implementation leading to the aforementioned behaviour can be found in [64]. Next, the second order convergence in time is clearly visible in the acoustic scaling, while the diffusive scaling works as first order in time (see Figure 10). Moreover, in the lower right corner of the landscape, the error caused by Euler's implementation is relatively small, thus it may not affect the order of convergence. Concluding, the same gain in accuracy can be accomplished along different pathways. The choice of the pathway will influence the computational cost. Based on this, one could select the spatio-temporal parameters of the simulation to progress along the iso-error line in order to obtain the desired result with a lower computational cost.

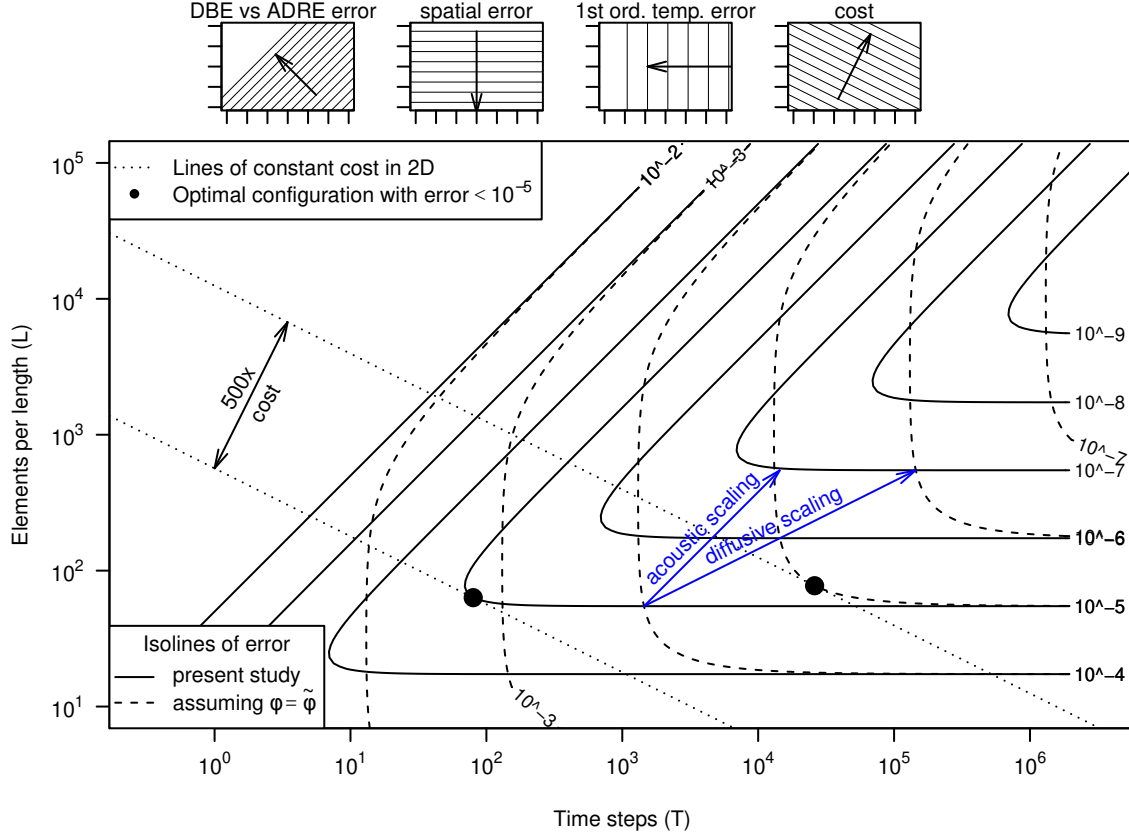


Figure 5: The schematic isolines of error in the T-L space. See Figure 4 for the plot of actual error, measured in simulation. First three of the top four plots show the trends of: error between discrete Boltzmann equation solution and advection-diffusion-reaction equation ($\sim (T/L)^{-2}$), error of the spatial discretisation ($\sim L^{-2}$), 1st order temporal error introduced by improper integration of the source term ($\sim T^{-1}$). The last of the top four plots presents the trend of the cost of the simulation for 2D lattice ($\sim L^2 T$). The large black circles mark optimal (CPU cheapest) selections of L and T to achieve the error of no more than 10^{-5} . The ratio of the computational cost for the optimal setup in the naive approach ($\phi = \tilde{\phi}$) compared to the present study is approximately 500 times. The vectors indicate the direction of spatio-temporal refinement using either acoustic or diffusive scaling. Assuming that the length of a vector corresponds to a single refinement step, the second order convergence can be deduced (as two iso-lines of errors are crossed) when looking at the diffusive scaling and setting $\phi = \tilde{\phi}$. In other words, the slope of convergence for diffusive scaling would be the same for both the proper and naive implementation.

4.2. The Allen-Cahn equation — illustrative advection-diffusion-reaction problem.

In this section a solidification problem was selected in order to illustrate the impact of the non-linear dependence of the source term on the transported scalar field. The problem solved is the Allen-Cahn equation in the form,

$$\frac{\partial \phi}{\partial t} + \nabla \cdot (\mathbf{u}\phi) = \nabla \cdot (M\nabla \phi) + \underbrace{\lambda\phi(1 - \phi^2)}_{Q=Q(\phi)}, \quad (34)$$

where the source term is responsible for the phase change. The details for this equation can be found in the dedicated literature, for example Cahn and Hilliard [65], Jacqmin [66]. To formulate the implicit relation between ϕ and $\tilde{\phi}$, the source term, $Q(\phi)$, was substituted into Equation (12),

$$\tilde{\phi} = \sum_i \tilde{h}_i = \phi - \frac{1}{2}Q(\phi) = \phi - \frac{1}{2}\lambda\phi(1 - \phi^2) = \phi\left(1 - \frac{\lambda}{2}(1 - \phi^2)\right). \quad (35)$$

As previously discussed, this equation has to be solved to express ϕ as a function of $\tilde{\phi} = \sum_i h_i$ to resolve the implicit relation introduced by $Q = Q(\phi)$. The exact solution can be readily derived for this third order polynomial. For $\lambda < 2$, there is only one real-valued solution,

$$\phi(\tilde{\phi}) = \frac{A}{C} - C, \text{ where } A = \frac{2 - \lambda}{3\lambda}, B = \frac{\tilde{\phi}}{\lambda}, \text{ and } C = \sqrt[3]{\sqrt{B^2 + A^3} - B}. \quad (36)$$

In the next sections, this analytical expression is used in the LBM collision operator to calculate ϕ , and $Q(\phi)$. Figure 6 illustrates the relationship between ϕ , Q and $\tilde{\phi}$. Two stable fixed points correspond to the roots of Q , present at $\phi = \tilde{\phi} = 1$ and -1 , and one unstable at 0. The round-off errors can cause the solution of Equation (35) to drift

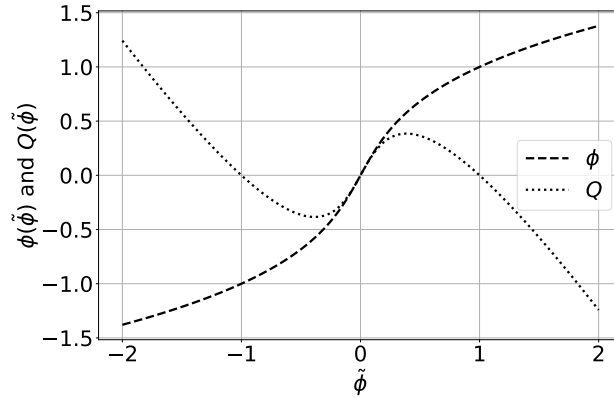


Figure 6: Plot presents the real solution of Equation (36), namely $\phi = \phi(\tilde{\phi})$ and $Q = Q(\tilde{\phi})$ for $\lambda = 1$.

from the unstable, 0, root (see Figure 6). Although direct implementation (as in the present work) of Equation (36) and calculation of the source term as $Q = Q(\phi) = \lambda\phi(1 - \phi^2)$ generates acceptable results, one can seek to improve the stability in two ways. In the first approach, an iterative (e.g. Newton-Raphson) method can be applied to find ϕ directly from Equation (35) instead of Equation (36). Then, $Q = Q(\phi)$ is calculated as before. Alternatively, ϕ and $\tilde{\phi}$ can be calculated from Equation (36) and Equation (35) respectively, while the source term (see Equation (12)) would correspond to double of their difference, $Q = 2(\phi - \tilde{\phi})$.

The following subsections are ordered by the growing complexity of benchmarks. First, only the reaction term is benchmarked. Then, a non-uniform initial condition is applied to observe the diffusive effects. Finally, an external velocity field is imposed to obtain the full advection-diffusion-reaction problem.

4.2.1. Uniform reaction benchmark — comparison with an analytical solution

This section analyses the evolution of a uniform initial distribution of the scalar field, ϕ , in the absence of an external velocity field. The spatial derivatives in Equation (34) reduce to zero and the problem simplifies to an ordinary differential equation,

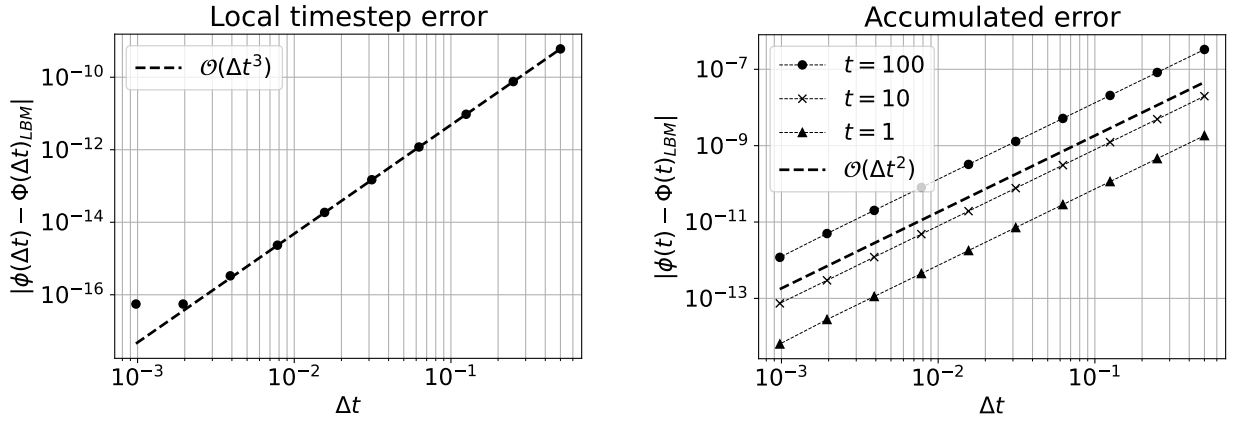
$$\frac{d\phi}{dt} = \lambda\phi(1 - \phi^2). \quad (37)$$

The analytical solution of this equation is,

$$\phi(t) = \pm \left(C_1 e^{-2\lambda t} + 1 \right)^{-\frac{1}{2}}, \text{ where } C_1 = (\phi(0))^{-2} - 1. \quad (38)$$

The results obtained from LBM using the Equation (36), were compared with the analytical solution of the ODE. In Figure 7, both local and global (accumulated) truncation errors are presented. The local time-step error was calculated as the difference between the numerical and analytical solution after a single time step. For this case, the third-order convergence up to the level of computational accuracy was recovered. As there is no diffusion, the Fourier number is undefined. The global convergence rate was determined by comparison of the numerical and analytical solution after a fixed time $t \in 1, 10, 100$. The coefficient responsible for the intensity of reaction was set to $\lambda = 0.01$.

As observed in Figure 7b, the scheme recovered the expected second-order convergence. From this result it can be concluded that the presented implementation recovers the trapezoidal integration scheme for the special case in which the Allen-Cahn partial differential equation reduces to an ODE.



(a) Local truncation error for a single time step. The error reaches 10^{-16} being the limit of numerical accuracy.

(b) Convergence of total/accumulated error, evaluated for three different times $t = 1; 10; 100$.

Figure 7: Convergence study of the reaction component of the Allen-Cahn Equation (34), on a $D2Q9$ lattice with uniform initial condition and on periodic domain with $\lambda = 0.01$. In such a case, the problem simplifies to an ODE given by Equation (37). The operator $|\bullet|$ on the vertical axis denotes a scalar absolute value. It is used to evaluate the error against the analytical solution. In general, a method which converges with $O(n + 1)$ local truncation error, has a global error of order $O(n)$. In this example, the convergence of a local time-step error is limited by truncation error at $\approx 10^{-16}$.

It is reminded that to obtain accurate solution, an accurate initialisation procedure which took into account the *shift* in calculated values (see Equation (13)) must be applied.

4.2.2. Reaction-diffusion benchmark (2D, periodic) — comparison with a finite-element solution

To ensure that the proposed collision kernel properly recovers the diffusion process, the LBM solver has been qualitatively compared against the finite element method (FEM). A spatially varying, periodic initial condition was applied on a square, unit domain using the exponential function,

$$\phi|_{t=0}(x, y) = \frac{1}{2e - e^{-1}} \left(e^{\sin(2\pi \frac{x}{L})} - 2e^{\sin(4\pi \frac{y}{L})} \right). \quad (39)$$

Figure 8a shows the result of the initialisation.

The FEM results were obtained using the FEniCS [67] solver. We used fourth-order Lagrange interpolation for spatial discretisation and fourth-order Runge-Kutta (ESDIRK43a) with adaptive time-stepping for time integration. The FEM was solved on a regular, triangular mesh in the 2D square domain of unit length. There were 25 divisions along each side of the domain resulting in $\sim 26^2$ elements in total. The time step ranged from approximately 10^{-4} to 10^{-5} . Diffusivity in FEM solver was set to one, while the reaction rate was defined by setting $\mathbf{Da} = 500$. The LBM domain was discretised with 256×256 lattice nodes and the diffusivity was set to $1/6$ in lattice units, and magic number was set to $1/12$. To match the solutions obtained by two different solvers, the results were reported for a specific non-dimensional time. There was no external velocity field, thus $\mathbf{Pe} = 0$.

Figure 8b provides a qualitative comparison between the FEM and LBM solutions at a time defined by $\mathbf{Fo} = 7.26 \times 10^{-3}$. Here, the colour contours from the FEM solution are aligned with the dashed iso-lines of the LBM solution. Figure 8c quantitatively compares the time evolution of the scalar field, ϕ , computed by both solvers, through the cross section denoted by the vertical dashed line in Figure 8a and Figure 8b. The initial condition, and three subsequent times are provided in the same figure. It can be clearly seen, that the LBM and FEM solutions agree.

4.2.3. Advection-diffusion-reaction benchmark (2D, periodic) — self-convergence study

This section investigates the convergence of the advection-diffusion-reaction problem, given by Equation (34). The exponential initial condition was used again, as per Equation (39). For this study, a TRT collision operator was used again, with the magic coefficient, Λ , set to $1/12$ in order to cancel out the third-order spatial error and provide optimal results for advection dominated problems [68]. The scalar field was advected with a uniform external velocity, U_x , corresponding to $\mathbf{Pe} = 1 \times 10^3$. The time of the simulation was determined by setting $\mathbf{Fo} = 1 \times 10^{-6}$. The Damköhler number has been set as $\mathbf{Da} = 1 \times 10^6$, to provide a scenario in which the reaction term dominates the diffusion behaviour. The convergence of the scheme was assessed using both acoustic and diffusive scaling techniques. The parameters used during these studies are provided in Table 2 and Table 3, respectively. Here, the number of elements per the domain length, L , is provided, as is the number of iterations, T .

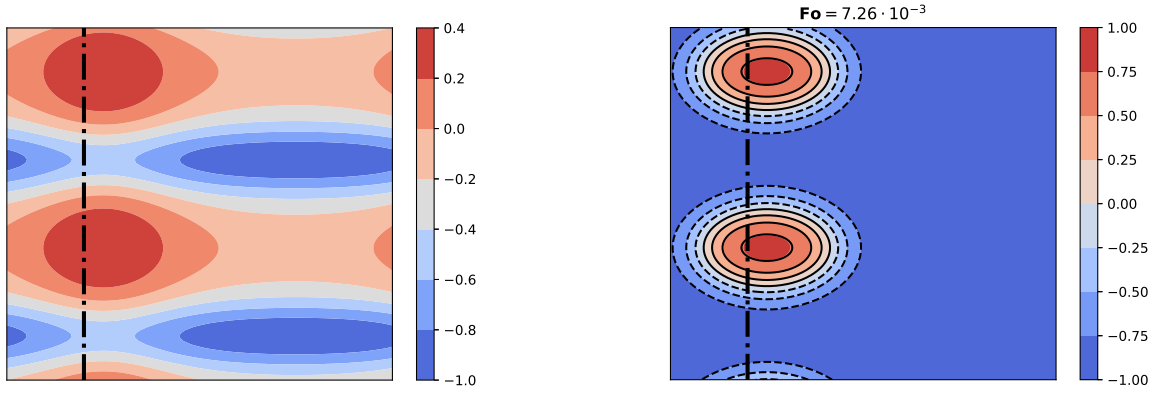
Table 2: Simulation parameters in lattice units, acoustic scaling, for $\mathbf{Pe} = 1 \times 10^3$, $\mathbf{Fo} = 1 \times 10^{-6}$ and $\mathbf{Da} = 1 \times 10^6$.

L	T	U_x	M	λ
4096	1024	4.00×10^{-3}	1.64×10^{-2}	9.77×10^{-4}
2048	512	4.00×10^{-3}	8.19×10^{-3}	1.95×10^{-3}
1024	256	4.00×10^{-3}	4.10×10^{-3}	3.91×10^{-3}
512	128	4.00×10^{-3}	2.05×10^{-3}	7.81×10^{-3}
256	64	4.00×10^{-3}	1.02×10^{-3}	1.56×10^{-2}

Table 3: Simulation parameters in lattice units, diffusive scaling, for $\mathbf{Pe} = 1 \times 10^3$, $\mathbf{Fo} = 1 \times 10^{-6}$ and $\mathbf{Da} = 1 \times 10^6$.

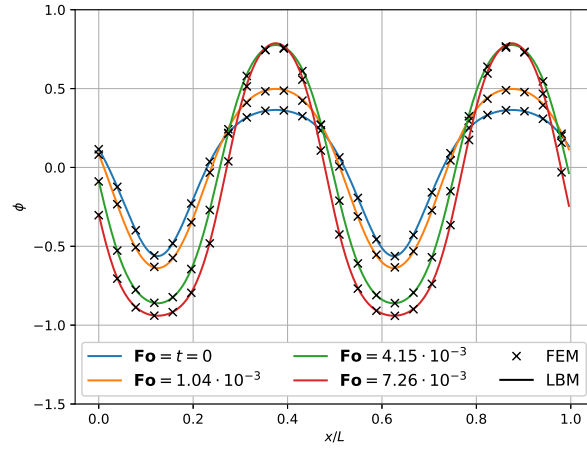
L	T	U_x	M	λ
4096	1024	4.00×10^{-3}	1.64×10^{-2}	9.77×10^{-4}
2048	256	8.00×10^{-3}	1.64×10^{-2}	3.91×10^{-3}
1024	64	1.60×10^{-2}	1.64×10^{-2}	1.56×10^{-2}
512	16	3.20×10^{-2}	1.64×10^{-2}	6.25×10^{-2}
256	4	6.40×10^{-2}	1.64×10^{-2}	2.50×10^{-1}

Figure 9 provides the result of the finest resolution simulated for the scalar variable, ϕ , and the implicit source term, $Q(\phi)$. As there does not exist an analytical solution to the complete advection-diffusion-reaction equation, this finest mesh solution is used to provide a reference point of convergence tests. The two scaling approaches (acoustic and diffusive) are evaluated in Figure 10 for both the proper and naive (assuming $\phi = \tilde{\phi}$) discretization of the source term, Q . The spatial and temporal resolutions are calculated as $\Delta x = 1/L$ and $\Delta t = 1/T$, respectively. In both scenarios, the proposed scheme provided second-order convergence with respect to the grid spacing. However, when



(a) The initial condition, given by Equation (39), used to initialize the intensity of the phase field, ϕ , for both the FEM and LBM solvers.

(b) The intensity of the phase field, ϕ , at the final time, $\mathbf{Fo} = 7.26 \times 10^{-3}$. Both FEM (colors) and LBM (lines) solutions are presented.



(c) The time evolution of the phase field, ϕ , is captured for four different Fourier numbers at a cross-section defined at $x/L = 0.2$. The FEM and LBM solutions are marked with crosses and lines respectively.

Figure 8: Comparison of the FEM and LBM solutions for reaction-diffusion problem specified in section 4.2.2. The LBM lattice consists of 256×256 nodes. Domain is periodic. The Péclet and Damköhler numbers are $\mathbf{Pe} = 0$, $\mathbf{Da} = 500$.

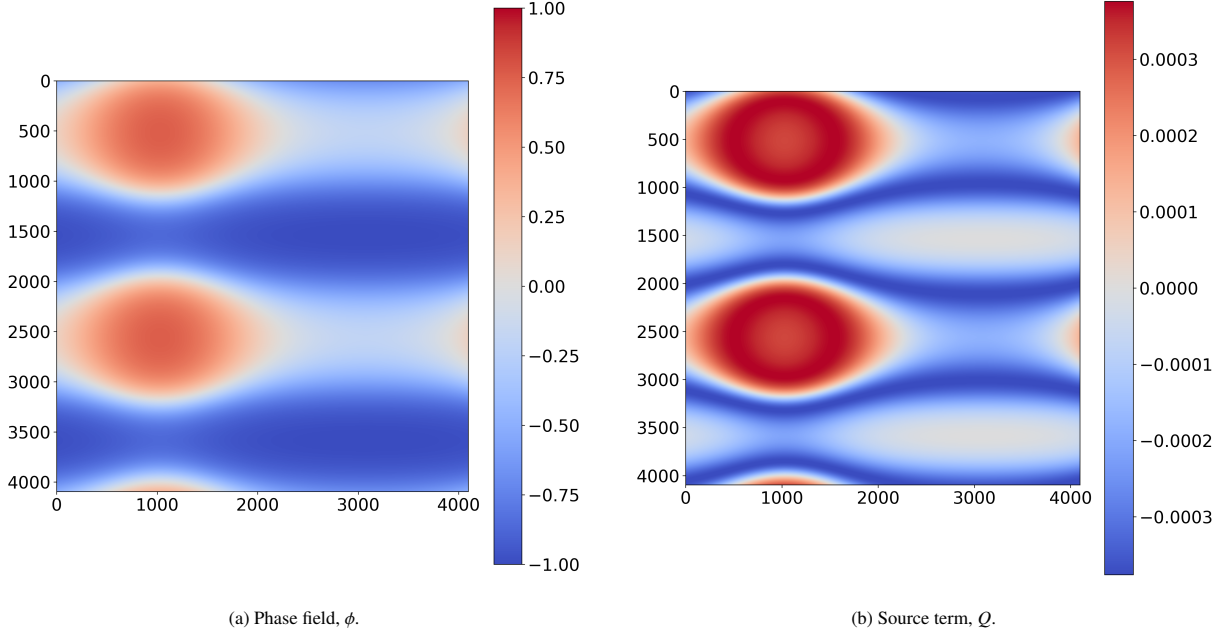
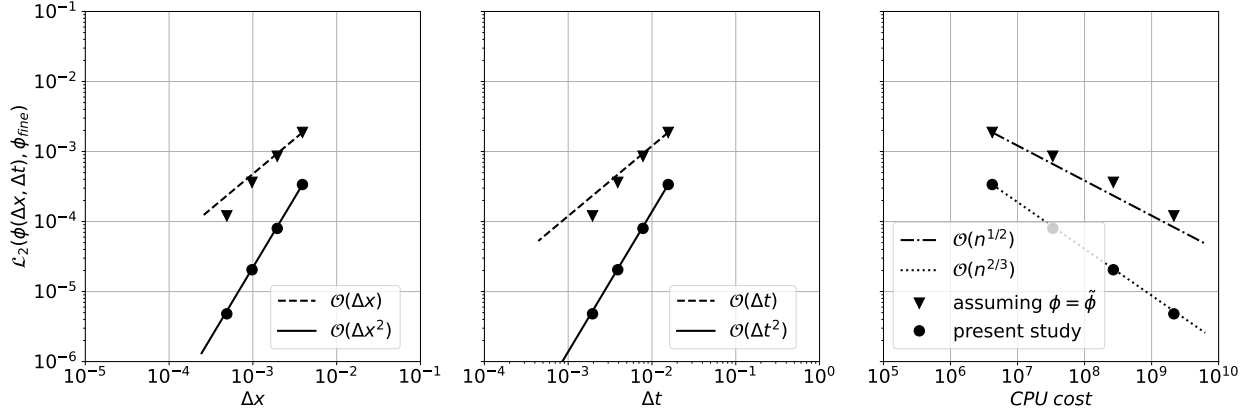


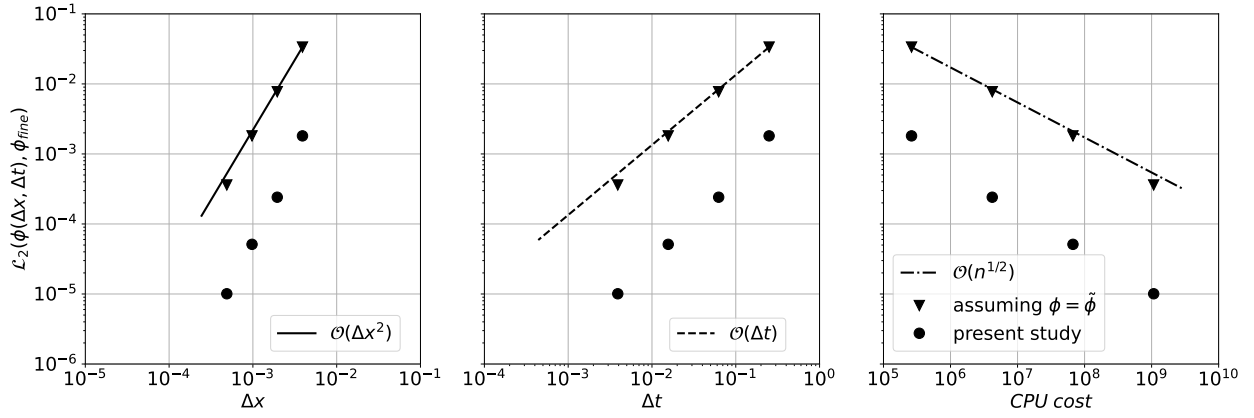
Figure 9: Contours of the reference solution on the 4096×4096 lattice, for $\mathbf{Pe} = 1 \times 10^3$, $\mathbf{Fo} = 1 \times 10^{-6}$ and $\mathbf{Da} = 1 \times 10^6$. The solver has been initialized according to Equation (39).

the diffusive scaling is applied, the spatial discretisation error dominates (see Fig. 5) which manifests as first-order dependence of the error on the time step. To understand the impact these convergence rates have in practice, the \mathcal{L}_2 error norm is shown as a function of the computational cost, defined as $CPU_{cost} = TL^2$, in Figure 10. Assuming that the simulation parameters will be maintained within the stability regime of the LBM (namely, $U_{max} \ll 0.1$, $\omega < 2$), one may conclude that for a given set of dimensionless numbers, it is more computationally effective to use acoustic scaling for mesh refinement, and diffusive scaling for mesh rarefaction. It is noted here, however, that a domain-specific simulation may affect the scaling approach. For example, one may prefer to use diffusive scaling in the simulation of flow through a porous medium as the effective boundary location is known to be affected by the choice of relaxation frequency [69, 70].

In addition to the above, the convergence rates reported in this test case highlight the importance of the error landscape previously introduced. The rates observed in Figure 10, indicate that the set of simulations were conducted below the diagonal of Figure 5. This apparent diagonal line sets the limit on the accuracy that could be obtained by means of a single acoustically scaled set of grids, and should be noted by practitioners looking to study the convergence of their LBM scheme. For the particular scenario investigated here, the temporal error dominates. By refining solely the time step, one can hide the source term discretization error below the spatial one and regain the second order convergence under acoustic scaling for the naive scheme.



(a) Acoustic scaling



(b) Diffusive scaling

Figure 10: Self-convergence study of an advection-diffusion-reaction Equation (34), on a $D2Q9$ lattice for $\mathbf{Pe} = 1 \times 10^3$, $\mathbf{Fo} = 1 \times 10^{-6}$ and $\mathbf{Da} = 1 \times 10^6$. Notice, that the formally second-order LBM scheme works as first-order with respect to time if the refinement is done along the diffusive pathway (see Section 4.1.3). Despite the same order of convergence under the diffusive scaling for both proper and naive (assuming $\phi = \tilde{\phi}$) discretization of the source term, the level of \mathcal{L}_2 error differs.

5. Conclusions

Since its initial formulation, the lattice Boltzmann method (LBM) has been developed and adapted to solve a variety of equations, addressing different physical scenarios. Current study has been focused on the details of the usage of LBM for advection-diffusion-reaction equation (ADRE) in which the source term directly depends on the advected field. Such source terms arise in the study of heat and mass transfer, phase-transition or evolution of species populations. Moreover most, implementations of immersed boundary method for heat flows, use source terms to account for desired thermal boundary conditions. In this paper, the state-of-the-art applications of the LBM for ADRE were presented, and the main differences in discretisation were discussed. A clear framework for derivation of the LBM numerical scheme from the discrete Boltzmann equation (DBE) was discussed, and the algebraic manipulations needed for it, were explicitly shown. Next, a simplification of the collision operator in the moments' space has been proposed.

The article reminds that an implicit relation (see Equation (12)) between the value of the macroscopic field and the zeroth-moment (sum) of the LBM densities is the key component for recovering the second-order convergence of the resulting LBM numerical scheme. Furthermore, the closed form solutions of this relation were presented for a variety of common source terms, ranging from simple linear terms to Gompertz model and the Allen-Cahn equation. Using this implicit relation, the paper presented a local and explicit single- or two relaxation time (TRT) LBM for ADRE with source terms dependent of the transported field.

To demonstrate the order of convergence of the proposed approach, two distinct equations, involving a linear source term, and a third-order one (as in the Allen-Cahn equation) were investigated. In the case of the linear source term, analytical solutions for both ADRE and DBE were obtained, allowing for the study of the dependence of the error of the LBM on both spatial and temporal resolution. This dependence was visualized as isolines, forming an error landscape. Different competing sources of error were discussed, as was the dependence of the convergence graph on choice of scaling and initial parameters. Moreover, by investigating the isolines of error one can find the point which minimizes the computational effort for a given accuracy. In the second benchmark, the relation between the macroscopic field and the shifted one was non-linear and implicit. The analytical solution was derived and embedded into the explicit, local evaluation of the LBM collision operator. The resulting numerical scheme was evaluated on three different test problems. Firstly, the domain was initialised with a uniform initial distribution to verify the accuracy of the time integration of the source term independently. The uniform initial distribution removed the spatial derivatives from the governing equation and allowed an analytical solution to be derived. In this scenario, the proposed scheme recovered the expected second-order global, and third-order local-in-time convergence. Next, the diffusion term was included in the assessment along with a periodic initial condition based on the exponential function. The result of a two-dimensional LBM simulation was compared to a fourth-order finite element method (FEM) solution, as an analytical solution for such case was no longer obtainable. Finally, to introduce advective effects an external velocity field was added to drive the phase field and a self-convergence study has been performed. The TRT collision operator was required to reduce the influence of numerical artefacts in the results.

All of the examples confirmed the consistency of the proposed approach and have shown the expected order of convergence. Observe, that the same implementation of the LBM scheme exhibits different order of convergence depending on the ratio of temporal and spatial refinements. For example, the formally second-order LBM scheme displays a first-order convergence with respect to time if the analysed with diffusive scaling (see Figure 10). Interestingly, in the case of this scaling, both the proper and naive (assuming $\phi = \tilde{\phi}$) discretizations will exhibit the same *slope* of convergence (see Figures 5 and 10), but the second-order scheme will result in the lower overall level of error. It is thus concluded that great care should be taken when verifying the order of the LBM scheme with tests of convergence.

6. Future Outlook

The same implicit relation of the macroscopic field to zeroth moment of the LBM densities, can be applied in the case of a system of ADRE, simply by replacing ϕ in Equation (12) by a vector of fields of interest. However, detailed analysis of the behaviour of the resulting LBM schemes is beyond the scope of this paper.

7. Declaration of Competing Interest

The authors declare that they have no known competing financial interests or personal relationships that could have appeared to influence the work reported in this paper.

8. CRediT authorship contribution statement

G. Gruszczyński: — Writing original draft, Review & Editing, Conceptualization, Methodology, Software, Data curation, Validation, Visualization, Formal analysis, Investigation.

M. Dzikowski — Formal analysis, Conceptualization, Investigation. [Appendix A](#), Sections 4.2.1 and 4.2.2 Writing, Software, Data curation, Validation, Visualization.

Ł. Łaniewski-Wołk — Formal analysis, Investigation. Table 1 and Section 4.1: Writing, Software, Data curation, Validation, Visualization.

9. Acknowledgements

Authors would like to acknowledge Travis Mitchell for proofreading of the manuscript and Jacek Szumbarski for insightful discussions. Numerical experiments were performed using computational resources provided by the Interdisciplinary Center for Mathematical and Computational Modelling of the University of Warsaw under grants GR80-12 and GR83-20. Work was supported by IDUB grant *Modelling of epidemic spreading with Lattice Boltzmann Method*, funded by Warsaw University of Technology. The simulations were completed using the open-source TCLB solver [71] available at: <https://github.com/CFD-GO/TCLB>

Appendix A. Example: Direct derivation of the 0D scheme from ODE

As an illustrative exercise, a direct derivation of numerical scheme for an ordinary differential equation (ODE), analogous to the proposed LBM scheme, is presented. Consider an ODE,

$$\frac{d}{dt}\phi = Q(\phi, t). \quad (\text{A.1})$$

Integrating it with the trapezoidal rule leads to the update formula,

$$\phi(t + \delta t) = \phi(t) + \frac{\delta t}{2} \left(Q(\phi(t), t) + Q(\phi(t + \delta t), t + \delta t) \right), \quad (\text{A.2})$$

which belongs to a wider class of implicit Adams-Moulton methods. Introduction of a $\frac{\delta t}{2}$ shift, similarly to the LBM derivation presented in Section 2.1,

$$\tilde{\phi} = \phi - \frac{\delta t}{2} Q \longrightarrow \phi = \tilde{\phi} + \frac{\delta t}{2} Q, \quad (\text{A.3})$$

allows to transform this update formula into an explicit one,

$$\tilde{\phi}(t + \delta t) + \frac{\delta t}{2} \cancel{Q(\phi(t + \delta t), t + \delta t)} = \tilde{\phi}(t) + \frac{\delta t}{2} Q(\phi(t), t) + \frac{\delta t}{2} \left(Q(t) + \cancel{Q(\phi(t + \delta t), t + \delta t)} \right), \quad (\text{A.4})$$

as long as the transformation between ϕ and $\tilde{\phi}$ is bijective. This lead to a numerical scheme, identical to one obtained in LBM methodology,

$$\tilde{\phi}(t + \delta t) = \tilde{\phi}(t) + \delta t Q(\phi(t), t) \quad \text{where} \quad \phi(t) = \tilde{\phi}(t) + \frac{\delta t}{2} Q(\phi(t), t). \quad (\text{A.5})$$

Appendix B. Notes on integration of the discrete Boltzmann equation

To ease the reading of the main text, some of the algebraic transformations are listed here. The substitutions can prove a useful reference for the reader, especially for newcomers, although similar derivations can be also found LBM textbooks [2].

Substituting Equation (9) into the left-hand side of Equation (8) and Equation (10) into the right-hand side of Equation (8) gives,

$$\begin{aligned}
 \tilde{h}_i(\hat{\mathbf{x}}, \hat{t}) &= \left[1 - \frac{1}{2\tau}\right] \frac{\tilde{h}_i(\mathbf{x}, t) + \frac{1}{2\tau} h_i^{\text{eq}}(\phi, u) + \frac{1}{2} q_i(\mathbf{x}, t)}{1 + \frac{1}{2\tau}} + \frac{1}{2\tau} h_i^{\text{eq}}(\phi, u) + \frac{1}{2} q_i(\mathbf{x}, t) \\
 &= \frac{1 - \frac{1}{2\tau}}{1 + \frac{1}{2\tau}} \left[\tilde{h}_i(\mathbf{x}, t) + \frac{1}{2\tau} h_i^{\text{eq}}(\phi, u) + \frac{1}{2} q_i(\mathbf{x}, t) \right] + \frac{1}{2\tau} h_i^{\text{eq}}(\phi, u) + \frac{1}{2} q_i(\mathbf{x}, t) \\
 &= \frac{2\tau - 1}{2\tau + 1} \left[\tilde{h}_i(\mathbf{x}, t) + \frac{1}{2\tau} h_i^{\text{eq}}(\phi, u) + \frac{1}{2} q_i(\mathbf{x}, t) \right] + \frac{1}{2\tau} h_i^{\text{eq}}(\phi, u) + \frac{1}{2} q_i(\mathbf{x}, t) \\
 &= \underbrace{\frac{2\tau - 1}{2\tau + 1}}_{F_1} \tilde{h}_i(\mathbf{x}, t) + \underbrace{\frac{1}{2\tau} \left[1 + \frac{2\tau - 1}{2\tau + 1}\right]}_{F_2} h_i^{\text{eq}}(\phi, u) + \underbrace{\frac{1}{2} \left[1 + \frac{2\tau - 1}{2\tau + 1}\right]}_{F_3} q_i(\mathbf{x}, t). \tag{B.1}
 \end{aligned}$$

Next, introducing the relaxation frequency, $\omega = \frac{1}{\tau + 1/2}$, simplifies the expressions further,

$$F_1 = \frac{2\tau - 1}{2\tau + 1} = \frac{2\tau + 1}{2\tau + 1} - \frac{2}{2\tau + 1} = 1 - \frac{1}{\tau + 1/2} = 1 - \omega. \tag{B.2}$$

$$F_2 = \frac{1}{2\tau} \left[1 + \frac{2\tau - 1}{2\tau + 1}\right] = \frac{1}{2\tau} \frac{4\tau}{2\tau + 1} = \frac{2}{2\tau + 1} = \omega. \tag{B.3}$$

$$F_3 = \frac{1}{2} \left[1 + \frac{2\tau - 1}{2\tau + 1}\right] = \frac{2\tau}{2\tau + 1} = \frac{2\tau + 1}{2\tau + 1} - \frac{2}{2\tau + 1} = 1 - \frac{1}{2} \omega. \tag{B.4}$$

Substituting Equations (B.2-B.4) into Equation (B.1), the desired Equation (11) emerges,

$$\tilde{h}_i(\mathbf{x} + \mathbf{e}_i, t + 1) = \tilde{h}_i^*(\mathbf{x}, t) = (1 - \omega) \tilde{h}_i(\mathbf{x}, t) + \omega h_i^{\text{eq}}(\phi, u) + \left(1 - \frac{\omega}{2}\right) q_i(\mathbf{x}, t). \tag{B.5}$$

Appendix C. Comparison of approaches to the source term integration

The appropriate integration of the DBE with the trapezoidal rule and redefinition of variables allows one to derive a second-order accurate, local, and explicit evolution scheme as presented in Equation (11). To broaden the discussion of approaches available in the literature, this appendix briefly analyses the spatio-temporal derivatives of the source term that appears in the works of Shi et al. [36, 42] and Chai et al. [37, 39]. If the source term is not included in the

shift of variables, then the evolution equation reads,

$$\bar{h}_i(\mathbf{x} + \mathbf{e}_i, t + 1) = \bar{h}_i^*(\mathbf{x}, t) = (1 - \omega)\bar{h}_i(\mathbf{x}, t) + \omega h_i^{\text{eq}}(\phi, \mathbf{u}) + q_i(\phi, \mathbf{x}, t) + \frac{1}{2} \left(\frac{\partial}{\partial t} + \mathbf{e}_i \cdot \nabla \right) q_i(\phi, \mathbf{x}, t), \quad (\text{C.1})$$

where contrary to the presented scheme, $\phi = \bar{\phi} = \sum_i \bar{h}_i$ and \bar{h} is a shifted variable, analogous to \tilde{h}_i , but without the contribution of q_i .

To understand the relation between Equation (C.1), and the one described in the present study (given by Equation (11)), consider the right hand side of Equation (5). The I_2 integral consist of two parts, first related to collision and second to the source term. In fact, any number of different numerical techniques can be applied to each of them. For example, instead of applying the trapezoidal rule, one can use a first order approximation of the source term,

$$\begin{aligned} q_i(\phi(\mathbf{x} + s\mathbf{e}_i, t + s), \mathbf{x} + s\mathbf{e}_i, t + s) &= q_i(\phi(\mathbf{x}, t), \mathbf{x}, t) + s \frac{\partial}{\partial s} (q_i(\phi(\mathbf{x} + s\mathbf{e}_i, t + s), \mathbf{x} + s\mathbf{e}_i, t + s)) + O(s^2) \\ &= q_i(\phi(\mathbf{x}, t), \mathbf{x}, t) + s \left(\underbrace{\frac{\partial t}{\partial s}}_{=1} \frac{\partial}{\partial t} + \underbrace{\frac{\partial \mathbf{x}}{\partial s}}_{=\mathbf{e}_i} \cdot \frac{\partial}{\partial \mathbf{x}} \right) q_i(\phi(\mathbf{x}, t), \mathbf{x}, t) + O(s^2) \\ &\simeq q_i(\phi(\mathbf{x}, t), \mathbf{x}, t) + s \left(\frac{\partial}{\partial t} + \mathbf{e}_i \cdot \nabla \right) q_i(\phi(\mathbf{x}, t), \mathbf{x}, t). \end{aligned} \quad (\text{C.2})$$

This approximation can be integrated giving,

$$\begin{aligned} \int_0^1 q_i(\phi(\mathbf{x} + s\mathbf{e}_i, t + s), \mathbf{x} + s\mathbf{e}_i, t + s) ds &= \left[s q_i(\phi(\mathbf{x}, t), \mathbf{x}, t) + \frac{s^2}{2} \left(\frac{\partial}{\partial t} + \mathbf{e}_i \cdot \nabla \right) q_i(\phi(\mathbf{x}, t), \mathbf{x}, t) + O(s^3) \right]_0^1 \\ &\simeq q_i(\phi, \mathbf{x}, t) + \frac{1}{2} \left(\frac{\partial}{\partial t} + \mathbf{e}_i \cdot \nabla \right) q_i(\phi, \mathbf{x}, t). \end{aligned} \quad (\text{C.3})$$

In the case of the *bottom-up* approach, the last term in Equation (C.3) is usually recognised as an artefact [21]. As pointed out by Seta [21], it can be removed by redefinition of variables or by addition of a correction with regard to the derivative of the source term. The derivative can be computed using a forward or backward finite difference (FD) expression. As one would expect, if a forward FD is used, then the result is equivalent to that obtained through the trapezoidal rule,

$$q_i(\phi, \mathbf{x}, t) + \frac{1}{2} \left(\frac{\partial}{\partial t} + \mathbf{e}_i \cdot \nabla \right) q_i(\phi, \mathbf{x}, t) = q_i(\phi, \mathbf{x}, t) + \frac{1}{2} (q_i(\hat{\phi}, \hat{\mathbf{x}}, \hat{t}) - q_i(\phi, \mathbf{x}, t)) = \frac{1}{2} (q_i(\hat{\phi}, \hat{\mathbf{x}}, \hat{t}) + q_i(\phi, \mathbf{x}, t)). \quad (\text{C.4})$$

The influence of the spatial component of the derivate, $\mathbf{e}_i \cdot \nabla$, and various FD stencils has been analysed in [42]. As long as the source term does not depend on ϕ , both forward and backwards FD are computationally trivial. However, if there is a dependence, the backwards FD would require additional transfer of data, while the forward FD, without the appropriate shift of variables, results in a globally implicit scheme.

References

- [1] X. He, S. Chen, G. D. Doolen, A Novel Thermal Model for the Lattice Boltzmann Method in Incompressible Limit, *Journal of Computational Physics* 146 (1998) 282–300.
- [2] T. Krüger, H. Kusumaatmaja, A. Kuzmin, O. Shardt, G. Silva, E. M. Viggen, *The Lattice Boltzmann Method*, 2017.
- [3] Y.-H. Fu, L. Bai, K.-H. Luo, Y. Jin, Y. Cheng, Modeling mass transfer and reaction of dilute solutes in a ternary phase system by the lattice boltzmann method, *Phys. Rev. E* 95 (2017) 043304.
- [4] C. Lin, A. Xu, G. Zhang, Y. Li, Double-distribution-function discrete Boltzmann model for combustion, *Combustion and Flame* 164 (2016) 137–151.
- [5] O. Aursjø, S. R. Pride, Lattice boltzmann method for diffusion-limited partial dissolution of fluids, *Phys. Rev. E* 92 (2015) 013306.
- [6] S. An, H. Erfani, H. Hellevang, V. Niasar, Lattice-boltzmann simulation of dissolution of carbonate rock during co2-saturated brine injection, *Chemical Engineering Journal* 408 (2021) 127235.

- [7] R. Huang, H. Wu, P. Cheng, A new lattice Boltzmann model for solid-liquid phase change, *International Journal of Heat and Mass Transfer* 59 (2013) 295–301.
- [8] R. Huang, H. Wu, Phase interface effects in the total enthalpy-based lattice Boltzmann model for solid-liquid phase change, *Journal of Computational Physics* 294 (2015) 346–362.
- [9] Z. Guo, C. Zheng, B. Shi, T. S. Zhao, Thermal lattice Boltzmann equation for low Mach number flows: Decoupling model, *Physical Review E - Statistical, Nonlinear, and Soft Matter Physics* 75 (2007) 1–15.
- [10] I. V. Karlin, D. Sichau, S. S. Chikatamarla, Consistent two-population lattice Boltzmann model for thermal flows, *Physical Review E - Statistical, Nonlinear, and Soft Matter Physics* 88 (2013) 1–13.
- [11] L. Fei, K. H. Luo, C. Lin, Q. Li, Modeling incompressible thermal flows using a central-moments-based lattice Boltzmann method, *International Journal of Heat and Mass Transfer* 120 (2018) 624–634.
- [12] L. Fei, K. H. Luo, Cascaded lattice Boltzmann method for incompressible thermal flows with heat sources and general thermal boundary conditions, *Computers and Fluids* 165 (2018) 89–95.
- [13] F. M. Elseid, S. W. Welch, K. N. Premnath, A cascaded lattice boltzmann model for thermal convective flows with local heat sources, *International Journal of Heat and Fluid Flow* 70 (2018) 279–298.
- [14] K. Salari, P. Knupp, Code verification by the method of manufactured solutions, Technical Report, Sandia National Lab.(SNL-NM), Albuquerque, NM (United States), 2000.
- [15] S. P. Dawson, S. Chen, G. D. Doolen, Lattice Boltzmann computations for reaction-diffusion equations, *The Journal of Chemical Physics* 98 (1993) 1514–1523.
- [16] R. Blaak, P. M. A. Slood, Lattice dependence of reaction-diffusion in lattice Boltzmann modeling, *Computer Physics Communications* 129 (2000) 256–266.
- [17] S. Hosseini, N. Darabiha, D. Thévenin, Lattice Boltzmann formulation for conjugate heat transfer in heterogeneous media, *International Journal of Heat and Mass Transfer* (2018) 906–919.
- [18] H. Karani, C. Huber, Lattice Boltzmann formulation for conjugate heat transfer in heterogeneous media, *Physical Review E - Statistical, Nonlinear, and Soft Matter Physics* 91 (2015) 1–12.
- [19] S. Chen, Y. Y. Yan, W. Gong, A simple lattice Boltzmann model for conjugate heat transfer research, *International Journal of Heat and Mass Transfer* 107 (2017) 862–870.
- [20] Q. Li, K. H. Luo, Q. J. Kang, Y. L. He, Q. Chen, Q. Liu, Lattice Boltzmann methods for multiphase flow and phase-change heat transfer, *Progress in Energy and Combustion Science* 52 (2016) 62–105.
- [21] T. Seta, Implicit temperature-correction-based immersed-boundary thermal lattice Boltzmann method for the simulation of natural convection, *Physical Review E - Statistical, Nonlinear, and Soft Matter Physics* 87 (2013) 63304.
- [22] H. K. Jeong, H. S. Yoon, M. Y. Ha, M. Tsutahara, An immersed boundary-thermal lattice Boltzmann method using an equilibrium internal energy density approach for the simulation of flows with heat transfer, *Journal of Computational Physics* 229 (2010) 2526–2543.
- [23] S. K. Kang, Y. A. Hassan, A comparative study of direct-forcing immersed boundary-lattice Boltzmann methods for stationary complex boundaries, *International Journal for Numerical Methods in Fluids* 66 (2011) 1132–1158.
- [24] S. K. Kang, Y. A. Hassan, A direct-forcing immersed boundary method for the thermal lattice Boltzmann method, *Computers and Fluids* 49 (2011) 36–45.
- [25] R. Huang, H. Wu, An immersed boundary-thermal lattice Boltzmann method for solid-liquid phase change, *Journal of Computational Physics* 277 (2014) 305–319.
- [26] Y. Hu, D. Li, S. Shu, X. Niu, Study of multiple steady solutions for the 2D natural convection in a concentric horizontal annulus with a constant heat flux wall using immersed boundary-lattice Boltzmann method, *International Journal of Heat and Mass Transfer* 81 (2015) 591–601.
- [27] Z. Wang, Y. Wei, Y. Qian, A simple direct heating thermal immersed boundary-lattice Boltzmann method for its application in incompressible flow, *Computers and Mathematics with Applications* 80 (2020) 1633–1649.
- [28] A. Eshghinejadfard, D. Thévenin, Numerical simulation of heat transfer in particulate flows using a thermal immersed boundary lattice Boltzmann method, *International Journal of Heat and Fluid Flow* 60 (2016) 31–46.
- [29] S. Karimnejad, A. Amiri Delouei, M. Nazari, M. M. Shahmardan, M. M. Rashidi, S. Wongwises, Immersed boundary—thermal lattice Boltzmann method for the moving simulation of non-isothermal elliptical particles, *Journal of Thermal Analysis and Calorimetry* 138 (2019) 4003–4017.
- [30] K. Suzuki, T. Kawasaki, N. Furumachi, Y. Tai, M. Yoshino, A thermal immersed boundary–lattice Boltzmann method for moving-boundary flows with Dirichlet and Neumann conditions, *International Journal of Heat and Mass Transfer* 121 (2018) 1099–1117.
- [31] D. Noble, J. Torczynski, A lattice-boltzmann method for partially saturated computational cells, *International Journal of Modern Physics C* 9 (1998) 1189–1201.
- [32] O. Aursjø, E. Jøtestuen, J. L. Vinningland, A. Hiorth, An improved lattice Boltzmann method for simulating advective diffusive processes in fluids, *Journal of Computational Physics* 332 (2017) 363–375.
- [33] O. Aursjø, E. Jøtestuen, J. L. Vinningland, A. Hiorth, On the inclusion of mass source terms in a single-relaxation-time lattice Boltzmann method, *Physics of Fluids* 30 (2018).
- [34] Q. Kang, P. C. Lichtner, D. Zhang, Lattice Boltzmann pore-scale model for multicomponent reactive transport in porous media, *Journal of Geophysical Research: Solid Earth* 111 (2006).
- [35] S. A. Hosseini, A. Eshghinejadfard, N. Darabiha, D. Thévenin, Weakly compressible Lattice Boltzmann simulations of reacting flows with detailed thermo-chemical models, *Computers and Mathematics with Applications* 79 (2020) 141–158.
- [36] B. Shi, Z. Guo, Lattice Boltzmann model for nonlinear convection-diffusion equations, *Physical Review E - Statistical, Nonlinear, and Soft Matter Physics* 79 (2009).
- [37] Z. Chai, B. Shi, Z. Guo, A Multiple-Relaxation-Time Lattice Boltzmann Model for General Nonlinear Anisotropic Convection–Diffusion Equations, *Journal of Scientific Computing* 69 (2016) 355–390.
- [38] H. Yoshida, M. Nagaoka, Multiple-relaxation-time lattice Boltzmann model for the convection and anisotropic diffusion equation, *Journal of*

- Computational Physics 229 (2010) 7774–7795.
- [39] Z. Chai, B. Shi, Multiple-relaxation-time lattice Boltzmann method for the Navier-Stokes and nonlinear convection-diffusion equations: Modeling, analysis, and elements, *Physical Review E* 102 (2020) 24–26.
 - [40] R. Fučík, R. Straka, Equivalent finite difference and partial differential equations for the lattice Boltzmann method, *Computers & Mathematics with Applications* 90 (2021) 96–103.
 - [41] S. Simonis, M. Frank, M. J. Krause, Constructing relaxation systems for lattice boltzmann methods, *Applied Mathematics Letters* 137 (2023) 108484.
 - [42] B. Shi, B. Deng, R. Du, X. Chen, A new scheme for source term in LBGK model for convection-diffusion equation, *Computers and Mathematics with Applications* 55 (2008) 1568–1575.
 - [43] Z. Guo, C. Zheng, B. Shi, Discrete lattice effects on the forcing term in the lattice Boltzmann method, *Physical Review E - Statistical Physics, Plasmas, Fluids, and Related Interdisciplinary Topics* 65 (2002) 6.
 - [44] X. He, X. Shan, G. D. Doolen, Discrete Boltzmann equation model for nonideal gases, *Physical Review E* 57 (1998) R13–R16.
 - [45] T. Lee, C.-L. Lin, A stable discretization of the lattice Boltzmann equation for simulation of incompressible two-phase flows at high density ratio, *Journal of Computational Physics* 206 (2005) 16–47.
 - [46] X. Guo, B. Shi, Z. Chai, General propagation lattice Boltzmann model for nonlinear advection-diffusion equations, *Physical Review E* 97 (2018) 043310.
 - [47] A. Krämer, D. Wilde, K. Küllmer, D. Reith, H. Foyi, W. Joppich, Lattice boltzmann simulations on irregular grids: Introduction of the natrium library, *Computers and Mathematics with Applications* 79 (2020) 34–54.
 - [48] D. Wilde, A. Krämer, K. Küllmer, H. Foyi, D. Reith, Multistep lattice boltzmann methods: Theory and applications, *International Journal for Numerical Methods in Fluids* 90 (2019) 156–169.
 - [49] D. Strzelczyk, M. Matyka, How nodes layout, refinement and velocity discretization influence convergence of the meshless lattice boltzmann method, *SSRN Electronic Journal* (2022).
 - [50] J. Wang, M. Wang, Z. Li, A lattice boltzmann algorithm for fluid-solid conjugate heat transfer, *International Journal of Thermal Sciences* 46 (2007) 228–234.
 - [51] B. Chopard, J. L. Falcone, J. Latt, The lattice Boltzmann advection-diffusion model revisited, *European Physical Journal: Special Topics* 171 (2009) 245–249.
 - [52] M. Geier, A. Greiner, J. G. Korvink, Cascaded digital lattice Boltzmann automata for high Reynolds number flow, *Physical Review E - Statistical, Nonlinear, and Soft Matter Physics* 73 (2006) 1–10.
 - [53] X. B. Nie, X. Shan, H. Chen, Galilean invariance of lattice Boltzmann models, *EPL* 81 (2008) 34005.
 - [54] A. De Rosi, K. H. Luo, Role of higher-order Hermite polynomials in the central-moments-based lattice Boltzmann framework, *Physical Review E* 99 (2019).
 - [55] A. L. Kupershtokh, D. A. Medvedev, D. I. Karpov, On equations of state in a lattice Boltzmann method, *Computers and Mathematics with Applications* 58 (2009) 965–974.
 - [56] L. Fei, K. H. Luo, Consistent forcing scheme in the cascaded lattice Boltzmann method, *Physical Review E* 96 (2017) 053307. Publisher: American Physical Society.
 - [57] R. Huang, H. Wu, N. A. Adams, Eliminating cubic terms in the pseudopotential lattice Boltzmann model for multiphase flow, *Physical Review E* 97 (2018) 53308.
 - [58] A. De Rosi, R. Huang, C. Coreixas, Universal formulation of central-moments-based lattice Boltzmann method with external forcing for the simulation of multiphysics phenomena, *Physics of Fluids* 31 (2019) 117102.
 - [59] G. Gruszczyński, T. Mitchell, C. Leonardi, T. Barber, et al., A cascaded phase-field lattice boltzmann model for the simulation of incompressible, immiscible fluids with high density contrast, *Computers & Mathematics with Applications* 79 (2020) 1049–1071.
 - [60] I. Ginzburg, Equilibrium-type and link-type lattice Boltzmann models for generic advection and anisotropic-dispersion equation, *Advances in Water Resources* 28 (2005) 1171–1195.
 - [61] A. Kuzmin, I. Ginzburg, A. A. Mohamad, The role of the kinetic parameter in the stability of two-relaxation-time advection-diffusion lattice Boltzmann schemes, *Computers and Mathematics with Applications* 61 (2011) 3417–3442.
 - [62] P. Asinari, Generalized local equilibrium in the cascaded lattice Boltzmann method, *Physical Review E - Statistical, Nonlinear, and Soft Matter Physics* 78 (2008) 1–5.
 - [63] H. P. Langtangen, G. K. Pedersen, *Scaling of Differential Equations*, Simula SpringerBriefs on Computing, Springer International Publishing, 2016.
 - [64] M. Zhang, W. Zhao, P. Lin, Lattice Boltzmann method for general convection-diffusion equations: MRT model and boundary schemes, *Journal of Computational Physics* 389 (2019) 147–163.
 - [65] J. W. Cahn, J. E. Hilliard, Free Energy of a Nonuniform System. I. Interfacial Free Energy, *The Journal of Chemical Physics* 28 (1958) 258–267.
 - [66] D. Jacqmin, Calculation of Two-Phase Navier–Stokes Flows Using Phase-Field Modeling, *Journal of Computational Physics* 155 (1999) 96–127.
 - [67] M. S. Alnæs, J. Blechta, J. Hake, A. Johansson, B. Kehlet, A. Logg, C. Richardson, J. Ring, M. E. Rognes, G. N. Wells, The fenics project version 1.5, *Archive of Numerical Software* 3 (2015).
 - [68] I. Ginzburg, Consistent lattice Boltzmann schemes for the Brinkman model of porous flow and infinite Chapman-Enskog expansion, *Physical Review E - Statistical, Nonlinear, and Soft Matter Physics* 77 (2008).
 - [69] C. Pan, L. S. Luo, C. T. Miller, An evaluation of lattice Boltzmann schemes for porous medium flow simulation, *Computers and Fluids* 35 (2006) 898–909.
 - [70] W. Regulski, J. Szumbariski, Łaniewski-WoŃk, K. Gumowski, J. Skibiński, M. Wichrowski, T. Wejrzanowski, Pressure drop in flow across ceramic foams-A numerical and experimental study, *Chemical Engineering Science* 137 (2015) 320–337.
 - [71] Ł. Łaniewski-WoŃk, J. Rokicki, Adjoint Lattice Boltzmann for topology optimization on multi-GPU architecture, *Computers and Mathematics with Applications* 71 (2016) 833–848.